Modeling Effects of Annealing on Coal Char Reactivity to O_2 and CO_2 Based on Preparation Conditions

Troy Holland,[1,2] Sham Bhat,[2] Peter Marcy,[2] James Gattiker,[2] Joel D. Kress,[2] and Thomas H. Fletcher*,[1]

[1] Chemical Engineering Dept., Brigham Young University, Provo, UT, USA 84602
[2]Los Alamos National Laboratory

*Corresponding author,

email: tom_fletcher@byu.edu,

phone: 1-801-422-6236

Abstract

Oxy-fired coal combustion is a promising potential carbon capture technology. Predictive CFD simulations are valuable tools in evaluating and deploying oxy-fuel and other carbon capture technologies either as retrofit technologies or for new construction. However, accurate predictive combustor simulations require physically realistic submodels with low computational requirements. A recent sensitivity analysis of a detailed char conversion model (Char Conversion Kinetics (CCK)) found thermal annealing to be an extremely sensitive submodel. In the present work, further analysis of the previous annealing model revealed significant disagreement with numerous data sets from experiments performed after that annealing model was developed. The annealing model was accordingly extended to reflect experimentally observed reactivity loss due to thermal annealing of a variety of coals in diverse char preparation conditions. The model extension was informed by a Bayesian calibration analysis. Additionally, because oxy-fuel conditions include extraordinarily high levels of CO_2, development of a first-ever CO_2 reactivity loss model due to annealing is presented.

Key Words: coal, char oxidation, oxy-fuel, kinetics, sensitivity analysis

Nomenclature

Parameter(s)	Description
a	A parameter for determining the mean of the annealing activation energy distribution
$A_{d,0}$	The initial value of A_d (s^{-1})
A_d	The preexponential factor of the annealing reaction (s^{-1})_
b	A parameter for determining the mean of the annealing activation energy distribution
B_f	A factor used to bifurcate the log normal distribution of the annealing activation energy
B_r	A factor used to bifurcate the log normal distribution of the annealing activation energy
c	A parameter for determining the mean of the annealing activation energy distribution
CBK	Carbon Burnout Kinetics model
CCK	Carbon Conversion Kinetics model
E_d	The activation energy of some thermal deactivation process (kcal/mol)
f	The fraction of carbon converted (burned) from the char, post devolatilization
f_i	The fraction of active sites in bin “i" in the thermal annealing model
HR	The *initial* particle heating rate (K/s)
HTT	The high temperature heat treatment time (s)
MC_R	Measured **relative** coal reactivity (post annealing)
PC_R	Model-predicted **relative** coal reactivity (post annealing)
p_0	An NMR parameter for the fraction of intact bridges in the coal pseudo monomer.
T_{peak}	Peak particle temperature during heating (K)
V_{ASTM}	ASTM volatile yield (wt% daf)
y	The prediction (with uncertainty) of the model+discrepancy+observational error
δ	The discrepancy between a model and reality, typically due to incomplete system knowledge or the ubiquitous, imperfect assumptions used to develop a model
ε	The observational error (noise) in experimental observations
η	The model (or an emulator thereof)
μ_{Ed}	The mean of the annealing activation energy distribution (kcal/mol)
σ_0	The initial standard deviation of the annealing activation energy distribution (kcal/mol)

σ_{Ed}	The standard deviation of the annealing activation energy distribution (kcal/mol)

1. Introduction

Pulverized coal combustion has accounted for the bulk of global electricity production for decades, and the increase in natural gas consumption notwithstanding, current outlooks indicate that coal-generated power will play a crucial role for the foreseeable future. As might be expected, coal dominates not only electricity generation, but also CO_2 emissions. If the industrialized world intends to meet targets for emissions reduction, carbon capture and sequestration methods are vital. Oxy-fired pulverized coal combustion is one potential piece of the carbon capture puzzle.

Oxy-fired combustion has been reviewed thoroughly elsewhere,[1, 2] but essentially involves a gas feed stream of high purity O_2 with the pulverized coal rather than the conventional air feed stream. In pure O_2, the gas temperatures become high enough to cause materials problems, so the flue gas is typically recycled, producing a local combustion environment that is highly enriched in CO_2, O_2, and (potentially) H_2O. Because the flue gas then has a very high CO_2 mole fraction (and essentially no N_2) it is relatively easy to capture prior to sequestration.

While the oxycoal design may facilitate carbon capture, it also dramatically alters the ambient conditions that coal particles experience. This dramatic shift in ambient atmosphere must be properly accounted for in models intended to predict oxy-coal design performance. A comprehensive single-particle coal combustion model (Carbon Conversion Kinetics or CCK) was recently subjected to a global sensitivity analysis.[3] The results indicated that the parameters

of the thermal annealing submodel were overwhelmingly the most sensitive of the parameter sets (relative to char burnout and temperature profile predictions) besides the chemical kinetic parameters. The analysis further concluded that the dominant annealing sensitivity was likely to be similar in other comparably detailed char combustion models. Based on this observation, the state of the art for coal char annealing models was examined, and extensions were explored to enable the CCK annealing submodel to capture the results of relevant data.

In the present work, thermal annealing is used as an umbrella term to include both the radical changes in char reactivity due to coal pyrolysis and the lesser (but still substantial) reactivity loss induced by thermal treatment of the post-pyrolysis char. These effects may include reactivity loss due to changes in coal morphology (swelling, changes in pore structure, molten ash that physically plugs pores) and a shift in coal chemistry (cross-linking, loss of reactive groups, rearrangement of char carbon structure, loss of inorganic catalytic activity etc.). Such a broad definition of annealing is adopted because, at the temperatures of practical coal combustion, it may well be infeasible to separate the numerous effects since they occur on similar time scales and may be better viewed as continuous rather than discrete events.[4]

2. Literature Observations

The impact of thermally-activated reactivity loss on carbon oxidation was observed decades ago.[5] Since then, numerous researchers have documented char reactivity loss, [6-13] and developed several models to incorporate variable char reactivity in combustion modeling. The available annealing literature spans an eclectic mix of carbon-based materials, preparation conditions, and char structural changes (both chemical and physical). Though the myriad processes of char

annealing are not fully understood, the literature on the subject makes several useful observations.

2.1. Annealing Time Scale

Senneca and Salatino[14] mapped relative reaction rates of pyrolysis, combustion, and post-pyrolysis combustion for a wide range of temperatures. Their work confirmed that pyrolysis is essentially complete by about 1200 K, well before post-pyrolysis annealing or combustion are of significant concern. They also found that annealing and combustion occur on similar time scales at around 1800 K. Finally, they showed that post-pyrolysis thermal annealing rates are rapid compared to combustion above about 1800 K, which implies that annealing is essentially complete before significant char oxidation occurs (at practical combustion conditions).

2.2. Impact of Reactive Gases

Senneca et al.[15-17] found that, when the char was heated and occasional puffs of O_2 were added to the system, annealing (as measured by crystallinity observed via HRTEM) was significantly inhibited if the heat treatment temperature was less than approximately 1473 K. The HRTEM further revealed that activated oxygen complexes would form on the carbon layers of the char, but would become more and more sparse at higher temperatures. They did not find a similar effect using CO_2 puffs instead of O_2.

2.3. **Annealing Regimes**

Senneca et al.[4] mapped deactivation regimes between 773 K and 2273 K, and found that pyrolysis and cross-linking of the carbon matrix occurred first, followed by higher activation energy changes in the carbon molecular structure. This evolving turbostratic structure proceeded in both series and parallel. Pyrolysis effects were dominant up to ~1000 K, loss of defects between carbon layers dominated between ~1000 and ~1800 K, decreased in-plane defects became important between ~1800 and ~2300 K, and crystallite growth occurred above ~2300 K. Naturally, each of these regimes contain numerous activated processes, resulting in a degree of overlap between regimes.

2.4. Char Precursor Impact

Annealing experiments yield somewhat different results for any two precursors, even when all other preparation conditions are held constant, i.e., no two coals anneal along exactly the same path. This is unsurprising, but conversely, many studies show that heat-treated chars do converge towards the same reactivity (i.e., that of graphite). Hurt and Gibbins[18] found that eight precursors all tended to converge in reactivity at high treatment temperatures, but the convergence was most marked in the residuals of actual boiler ash. The authors suggested (very plausibly in light of the general literature trends) that this greater convergence and annealing of char was due to the intense boiler conditions.

2.5. Heating Rate Impact

Cai et al.[19] studied the impact of heating rate on various precursors, holding other preparation conditions fixed, and found that precursors with high tar yield were quite sensitive to heating rates between very low heating rates (ca. 1 K/s) up to intermediate heating rates of ~1000 K/s, with a plateau above about 1000 K/s. These chars showed a substantial *increase* in reactivity, and the authors theorized that this was due to the enhanced porosity that softening, high volatile coals experience with rapid devolatilization, and that there is an upper limit to this enhancement.

2.6. Peak Temperature Impact

Shim and Hurt[20] observed that the peak temperature experienced by a char particle almost entirely dictates the degree of char annealing for a given precursor and heating rate. This is certainly due in part to the exponential temperature dependence of the annealing rate, but several effects fundamentally alter the distribution of available annealing processes, and can also be included in a T_{peak} effect. Such effects include whether or not ash fusion temperatures were reached (which affects catalysis for both char conversion and rearrangement[21-24]), or if the particle temperature was sufficient to prevent a high concentration of O_2 complexes from forming on the char surface.[17] For practical purposes, many of the effects based on peak temperature are irrelevant or complete at high heating rates and temperatures above about 1500 K. Because many of the relevant data points were taken in the high heating rate/high temperature region, and because ash content is diverse between coals, the data may be

insufficient to fully capture alterations to the annealing activation energy distribution based on $T_{peak.}$

2.7. Annealing Impacts *only* the Preexponential Factor

Salatino et al.[25] found that, under a broad range of preparation conditions, the activation energy of the gasification reaction remains essentially constant, and the preexponential factor alone is altered by the heat-treatment time-temperature profile.

2.8. Annealing Impact on both the CO_2 and the O_2 Reaction

Historically, the annealing model has impacted CO_2, H_2O, and O_2 reaction rates with a single, shared annealing factor derived in the CBK code and included in the more recent CCK code.[26-28] To the author's knowledge, no comprehensive char conversion model has ever employed distinct annealing mechanisms and submodels for conversion due to O_2 vs CO_2, or even determined whether or not such a distinction is necessary. Because the oxy-coal system includes very high CO_2 concentrations, CO_2 gasification is not necessarily a negligible reactant, and the highly sensitive annealing model must be able to accommodate any differences implied by thermal deactivation data. The literature is ambiguous on whether or not O_2 and CO_2 annealing may proceed along different pathways. For example, Liu and Niksa[29] observed that distinct reactive intermediaries were necessary for CO_2 and O_2 reaction schemes. On the other hand Feng et al.[30] determined via XRD (x-ray diffraction crystallography) and HRTEM (high-resolution tunneling electron microscope) that, on the microstructural level at least, coal chars gasify in the same manner for conversion in both air and CO_2.

3. Experimental

The annealing model employed in CBK has been frequently reused in comprehensive char conversion models. The CBK annealing model was first calibrated to the relative paucity of experimental data available at the time, i.e., five papers published between 1973 and 1996 [6, 7, 9, 31, 32] The older data taken over a large time span resulted in highly diverse experimental methods, making it quite difficult to arrive at a single, consistent comparison. For example, particle sizes varied greatly, the reaction regime may have been zone I or zone II,[33] measures of reactivity were not uniform, treatment temperatures were generally hundreds of Kelvin lower than practical combustion conditions, and some of the precursors were carbon sources other than coal. Also, except for the most recent paper listed,[6] the data were obtained using exceptionally low heating rates (well below 1 K/s) and long heat treatment times (up to 2 hours). These data are potentially useful for the regimes they were taken in, but more recent data show clearly that the most dramatic and dynamic annealing occurs in the first tens or hundreds of milliseconds, implying that annealing models should focus on (or at least include) short timescale data. Fortunately, much data has been collected on the millisecond to second timescale in the two decades since Hurt et al.[28] published the CBK model. Unfortunately, the bulk of these data lack one or more crucial model input or output, such as a reasonably well-defined heating rate, comparable reactivity measurements, or a recorded proximate and ultimate analysis, etc. Nevertheless, the literature contains several times more applicable data now than at the advent of the CBK model, which implies the potential for a more broadly applicable, less uncertain annealing model. The data discussed here were obtained from a detailed search of the literature. Because the data fill an undesirably large table, only a small sampling of the data are presented here. However, because

the conversion of graphical data to a tabulated format entailed considerable effort and is likely of great value to related model development, the tables are made available elsewhere.[34]

3.1. Data for Annealed Char Reacting with O2

The bulk of available char annealing data pertain to the reactivity of annealed char in O_2. The relevant experiments were carefully designed to take reactivity data in zone I to examine the intrinsic reactivity of various annealed chars in a broad range of preparation conditions. All of the data listed below included a proximate and ultimate analysis (see Table 1) as well as details on the *initial* heating rate (HR, or heating rate of the coal particle in K/s) of the coal particles, the peak temperature achieved (T_p) , and the high temperature treatment time (HTT). In addition, annealing models require a reference char to calculate the relative loss of activity; thus, Table 2 includes similar data for the reference char as well. The data table also includes the measured char **relative** reactivity (MC_R), the **relative** char reactivity predicted by the model (PC_R), and a calculated value for p_0 (a chemical structure parameter from NMR spectroscopy discussed in the model development section and obtained from a correlation detailed elsewhere).[35] Because the reactivities are relative to some reference char, they are unitless. Again, due to space constraints Table 2 contains only a fraction of the data, much of which was used to generate a relevant selection of figures in the results and discussion section. The balance of the data are available elsewhere.[34]

Note that there are a number of char PC_R and MC_R (predicted and measured relative reactivity values) char values that are greater than 1. This is because the annealing decreases the reactivity by different amounts depending on time temperature profile, heating rate, peak particle

temperature and precursor. Thus, even within a single precursor, there is not always an unambiguously most extreme annealing condition to choose as the reference char. However, the modeling results and optimization proceed identically regardless of this idiosyncrasy.

Table 1. Ultimate analysis and ASTM volatiles for annealed char precursors in O_2 (wt% daf).

Coal Name	C	H	O	N	S	V_{ASTM}
Beulah Zap [20]	73.2	4.4	20.6	1	0.82	42
Pocahontas [20]	89.8	5	3.4	1.2	0.78	19.2
Illinois 6 [20]	78.2	5.5	9.8	1.3	5.4	45.5
South African [16]	80.66	4.51	12.69	1.46	0.73	27.4
Cerrejon [36]	81.76	5.15	11.91	1.82	0.75	40.13
Pocahontas [37]	91.81	4.48	1.66	1.34	0.51	19.54
Pittsburgh 8 [37]	84.95	5.43	6.9	1.68	0.91	41.7
Tillmanstone [19]	91.4	4.4	2.2	1.3	0.7	18.1
Pittsburgh 8 [19]	83.2	5.3	9	1.6	0.9	41.7
Lindby [19]	81	5.3	11	1.7	1	37.5
Illinois 6 (APCS)[19]	77.7	5	13.5	1.4	2.4	47.4
Illinois 6 (SBN)[19]	75.6	5.8	14.5	1.4	2.7	47
South African [38]	80.66	4.51	12.69	1.46	0.73	27.4
High Volatile Bituminous [39]	80.33	5.95	10.97	1.44	0.96	44.43
Pittsburgh 8 [40-42]	84.95	5.43	6.9	1.68	0.91	41.7
Blind Canyon [40-42]	81.32	5.81	10.88	1.59	0.37	48.11
Beulah Zap [40-42]	74.05	4.9	19.13	1.17	0.71	49.78
South African [11]	82.5	4.6	13.2	1.46	0.73	27.43
South African [25]	82.66	4.51	12.69	1.46	0.73	27.4
Shenfu [43]	80.14	5.52	12.29	1.83	0.22	40.64
Rhur [22]	81.03	5.03	10.48	2.1	1.2	32.91
South African [38]	80.66	4.51	12.69	1.46	0.73	27.4
High Ash Indian [44]	72.82	4.65	19.91	1.79	0.83	50.03

Table 2. Detailed Experimental Data for Annealing Effects on Char Reactivity in O_2

Coal name	PC_R	MC_R	p_0	HR (K/s)	T_p (K)	HTT (s)	Ref HR (K/s)	Ref T_p (K)	Ref HTT (s)
Beulah Zap	3.23	25.7	0.65	1e5	1514	2	1e5	2295	2
Beulah Zap	2.24	22.2	0.65	1e5	1735	2	1e5	2295	2

Beulah Zap	1.68	15.0	0.65	1e5	1925	2	1e5	2295	2
Beulah Zap	1.33	6.70	0.65	1e5	2086	2	1e5	2295	2
Pocahontas	3.69	22.6	0.70	1e5	1606	2	1e5	2388	2
Pocahontas	2.55	6.12	0.70	1e5	1809	2	1e5	2388	2
Pocahontas	2.16	2.68	0.70	1e5	1903	2	1e5	2388	2
Pocahontas	1.73	1.43	0.70	1e5	2032	2	1e5	2388	2
Pocahontas	1.44	1.06	0.70	1e5	2152	2	1e5	2388	2
Pocahontas	1.12	1.00	0.70	1e5	2315	2	1e5	2388	2
Illinois 6	1.56	42.5	0.45	1e5	1585	2	1e5	2155	2
Illinois 6	1.39	31.3	0.45	1e5	1731	2	1e5	2155	2
Illinois 6	1.25	15.5	0.45	1e5	1857	2	1e5	2155	2
Illinois 6	1.16	6.94	0.45	1e5	1957	2	1e5	2155	2
Illinois 6	1.10	2.68	0.45	1e5	2006	2	1e5	2155	2
South African	1.25	2.08	0.67	16.7	1514	120	16.7	1503	1800
South African	1.22	1.29	0.67	16.7	1465	1800	16.7	1503	1800
South African	1.29	1.61	0.67	16.7	1438	1800	16.7	1503	1800
South African	2.17	6.02	0.67	16.7	1173	1800	16.7	1503	1800
South African	2.86	10.4	0.67	16.7	1173	60	16.7	1503	1800
Pocahontas	1.46	1.68	0.75	1e4	2073	0.15	1e4	2073	2
Pocahontas	1.23	1.13	0.75	1e4	2073	0.5	1e4	2073	2
Pocahontas	8.43	2.92	0.75	1e4	1273	0.15	1e4	2073	2
Pocahontas	7.27	2.15	0.75	1e4	1273	0.5	1e4	2073	2
Pocahontas	6.18	1.61	0.75	1e4	1273	2	1e4	2073	2
Pocahontas	5.55	1.55	0.75	1e4	1273	5	1e4	2073	2
Pocahontas	3.12	1.80	0.75	1e4	1673	0.15	1e4	2073	2
Pocahontas	2.64	1.41	0.75	1e4	1673	0.5	1e4	2073	2
Pocahontas	2.19	1.39	0.75	1e4	1673	2	1e4	2073	2
Pocahontas	1.93	1.31	0.75	1e4	1673	5	1e4	2073	2
Pocahontas	2.11	2.12	0.75	1e4	1873	0.15	1e4	2073	2
Pocahontas	1.77	1.34	0.75	1e4	1873	0.5	1e4	2073	2
Pocahontas	1.46	1.20	0.75	1e4	1873	2	1e4	2073	2
Pocahontas	1.29	1.09	0.75	1e4	1873	5	1e4	2073	2
Pittsburgh 8	1.22	1.49	0.52	1e4	2073	0.15	1e4	2073	2
Pittsburgh 8	1.12	1.12	0.52	1e4	2073	0.5	1e4	2073	2
Pittsburgh 8	2.89	5.46	0.52	1e4	1273	0.15	1e4	2073	2
Pittsburgh 8	2.67	4.53	0.52	1e4	1273	0.5	1e4	2073	2
Pittsburgh 8	2.44	2.78	0.52	1e4	1273	2	1e4	2073	2
Pittsburgh 8	2.29	2.79	0.52	1e4	1273	5	1e4	2073	2
Pittsburgh 8	1.82	3.08	0.52	1e4	1673	0.15	1e4	2073	2
Pittsburgh 8	1.69	2.33	0.52	1e4	1673	0.5	1e4	2073	2
Pittsburgh 8	1.50	2.08	0.52	1e4	1673	2	1e4	2073	2
Pittsburgh 8	1.42	2.03	0.52	1e4	1673	5	1e4	2073	2

Pittsburgh 8	1.48	2.84	0.52	1e4	1873	0.15	1e4	2073	2
Pittsburgh 8	1.37	2.03	0.52	1e4	1873	0.5	1e4	2073	2
Pittsburgh 8	1.21	1.39	0.52	1e4	1873	2	1e4	2073	2
Pittsburgh 8	1.15	1.30	0.52	1e4	1873	5	1e4	2073	2
Tillmanstone	0.77	0.63	0.77	5	1223	5	5e3	1223	5
Tillmanstone	0.98	0.90	0.77	1e3	1223	5	5e3	1223	5
Pittsburgh 8	1.47	3.34	0.53	1e3	973	2	5e3	1273	2
Pittsburgh 8	1.13	2.17	0.53	1e3	1173	2	5e3	1273	2
Pittsburgh 8	0.99	0.80	0.53	1e3	1273	2	5e3	1273	2
Pittsburgh 8	0.79	0.34	0.53	1e3	1473	2	5e3	1273	2
Pittsburgh 8	0.53	0.14	0.53	1e3	1773	2	5e3	1273	2
Pittsburgh 8	0.83	0.68	0.53	5	1273	2	5e3	1273	2
Pittsburgh 8	0.93	0.77	0.53	50	1273	2	5e3	1273	2
Linby	1.31	2.67	0.54	1e3	973	2	5e3	1273	2
Linby	1.11	1.92	0.54	1e3	1173	2	5e3	1273	2
Linby	0.98	0.97	0.54	1e3	1273	2	5e3	1273	2
Linby	0.77	0.47	0.54	1e3	1473	2	5e3	1273	2
Linby	0.44	0.10	0.54	1e3	1773	2	5e3	1273	2
Linby	0.75	0.50	0.54	2	1273	2	5e3	1273	2
Linby	0.91	0.86	0.54	50	1273	2	5e3	1273	2
South African	5.63	11.51	0.67	15	973	1200	16700	2273	2
South African	4.58	6.58	0.67	15	1173	60	16700	2273	2
South African	2.03	4.19	0.67	167	1473	1800	16700	2273	2
South African	1.21	3.32	0.67	167	1673	1800	16700	2273	2

The data used to calibrate the model were required to have a reactivity measurement that could be legitimately compared to the entire data set, which most commonly meant that the reactivity was given as a rate of change of normalized mass (i.e., the derivative of the degree of carbon conversion, f, with respect to time). Ideally, a complete particle time-temperature profile during heat-up would also be available, but given the extremely short time scale of many of the data points, it is not generally possible to solve the relevant energy balance to such a high level of precision. Instead, the estimated initial heating rate is used, as is common practice in coal-related

models that involve heating rate as a parameter. Finally, the data were generally taken between 30 and 70 % char conversion (i.e., after devolatilization).

The 70 % conversion boundary was chosen because the later stages of burnout are not fully understood. Senneca et al.[22] observed that particle reactivity from different particle preparation conditions often converged in late-stage burnout, while Hurt et al.[28] noted that burnout rates changed dramatically in the final ~15% of char consumption. This may be due to factors such as complete annealing, ash inhibition, rising experimental uncertainty near complete burnout, or a small fraction of exceptionally inert macerals. A full discussion of these effects is beyond the scope of the present work, but in all cases, late-stage burnout data is likely to include non-annealing effects. Alternatively, if annealing really is complete, then there is no purpose in training an annealing model to match irrelevant data. However, this seems unlikely to be the case, given that the annealed chars have never been observed to anneal to a perfect graphite crystal. Also, the trend of convergent reactivities is more based on extent of conversion rather than any factors expected to influence annealing, and the reactivity measurements are made at temperatures much lower than the heat-treatment, which implies very little further annealing during the low-temperature burnout.

As for the lower bound, the annealing model was trained only to data of at least 30% conversion, where char conversion begins to be measured post-pyrolysis. The first 30% of conversion data is excluded due to observed “early-stage” effects. The data show a trend of initially increasing reactivity, regardless of preparation conditions, in the first few percent of conversion, with a peak typically at ~20-30% carbon conversion. This could be due to plugged pores reopening,

adsorbed oxygen complexes releasing from the surface, highly reactive tar that had redeposited on the char surface, a peak in char surface area as pores expand, or a combination of many factors. This early stage is not well explored, and is complicated by numerous effects, so it was deemed inappropriate to select “early-stage” data for the training set.

As a final note on data selection, a few of the data sources included numerous data points at a single preparation condition. Rather than give this handful of experiments undue statistical weight, the replicate points were averaged together. This could be considered poor statistical practice in that a portion of the data is eliminated, but in this case the wide variety of data collection systems certainly introduces various biases that the model cannot (and should not) take into account. An overwhelming number of data points with a particular bias is therefore likely to prove detrimental to the model overall, even though the replicates would prove informative about the variance within that single experiment.

3.2. The Error Factor

To accurately assess model success, a quantity termed the “error factor” is defined. The error factor is the larger of the ratio of model prediction to experimental measurement or the reciprocal of that same ratio. The result is the factor by which the prediction differs from the measurement, and by taking the larger value, under-prediction is treated on equal footing with over-prediction (i.e., a ratio of PC_R/MC_R of 0.1 or 10 are both penalized as being off by a full order of magnitude).

3.3. Data for Annealed Char Reacting with CO_2 or H_2O

In recent years, thermal deactivation of coal char with respect to CO_2 and H_2O has garnered some interest. Annealing data relevant to gasification are still in the minority, but those rate data that met the same criteria as the analogous O_2 rate data are given below. Almost all of the data are for CO_2 reactivity, but the set from Jayamaran et al.[44] includes a handful of experiments with steam. Table 3 contains the relevant proximate and ultimate analysis, while Table 4 contains a selection of CO_2 and H_2O reactivity and preparation condition data. As before, Table 4 contains only a subset of the data, and additional data set was compiled, tabulated, and made available elsewhere.[34]

Table 3. Ultimate Analysis and ASTM Volatiles for Annealed Char Precursors in CO_2 and H_2O

Coal Name	Carbon %	Hydrogen %	Oxygen %	Nitrogen %	Sulfur %	ASTM Volatile %
South African[11]	82.5	4.6	13.2	1.46	0.73	27.43
South African[25]	82.66	4.51	12.69	1.46	0.73	27.4
Shenfu[43]	80.14	5.52	12.29	1.83	0.22	40.64
Rhur[22]	81.03	5.03	10.48	2.1	1.2	32.91
South African[38]	80.66	4.51	12.69	1.46	0.73	27.4
High Ash Indian[44]	72.82	4.65	19.91	1.79	0.83	50.03

Table 4. Detailed Experimental Data for Char Reactivity in CO_2 and H_2O

Coal name	PC_R	MC_R	p_0	HR (K/s)	T_p (K)	HTT (s)	Ref HR (K/s)	Ref T_p (K)	Ref HTT (s)
Shenfu	1.73	1.30	0.51	0.1	1223	1200	1e3	1773	1202
Shenfu	1.65	1.20	0.51	0.1	1273	1200	1e3	1773	1202
Shenfu	0.99	0.20	0.51	0.1	1673	1200	1e3	1773	1202
Shenfu	0.99	0.31	0.51	0.1	1673	1200	1e3	1773	1202
Shenfu	1.99	1.90	0.51	1e3	1223	1202	1e3	1773	1202

Shenfu	1.86	0.53	0.51	1e3	1273	1202	1e3	1773	1202
South African	4.58	5.17	0.67	15	1173	60	16700	2273	2
South African	4.58	4.50	0.67	15	1173	60	16700	2273	2
South African	2.03	2.31	0.67	167	1473	1800	16700	2273	2
South African	2.03	2.31	0.67	167	1473	1800	16700	2273	2
South African	2.03	2.09	0.67	167	1473	1800	16700	2273	2
South African	1.21	1.12	0.67	167	1673	1800	16700	2273	2
South African	1.21	0.93	0.67	167	1673	1800	16700	2273	2
South African	1.21	0.95	0.67	167	1673	1800	16700	2273	2
Indian	0.93	0.95	0.60	0.667	1273	300	13.3	1273	300
Indian	0.94	1.05	0.60	1.667	1273	300	13.3	1273	300
Indian	0.99	1.09	0.60	8.33	1273	300	13.3	1273	300
Indian	0.95	1.48	0.60	0.667	1173	300	13.3	1173	300
Indian	0.96	1.16	0.60	1.667	1173	300	13.3	1173	300
Indian	0.99	1.10	0.60	8.33	1173	300	13.3	1173	300
Indian	0.93	1.00	0.60	0.667	1223	300	13.3	1223	300
Indian	0.95	1.07	0.60	1.667	1223	300	13.3	1223	300
Indian	0.99	1.10	0.60	8.33	1223	300	13.3	1223	300
Indian	0.93	1.02	0.60	0.667	1273	300	13.3	1273	300
Indian	0.94	1.06	0.60	1.667	1273	300	13.3	1273	300
Indian	0.99	0.99	0.60	8.33	1273	300	13.3	1273	300
Indian	0.95	0.83	0.60	0.667	1173	300	13.3	1173	300
Indian	0.96	0.79	0.60	1.667	1173	300	13.3	1173	300
Indian	0.99	0.75	0.60	8.33	1173	300	13.3	1173	300
Indian	0.93	0.90	0.60	0.667	1223	300	13.3	1223	300
Indian	0.95	0.97	0.60	1.667	1223	300	13.3	1223	300
Indian	0.99	1.05	0.60	8.33	1223	300	13.3	1223	300
Indian	0.93	0.70	0.60	0.667	1273	300	13.3	1273	300
Indian	0.94	0.91	0.60	1.667	1273	300	13.3	1273	300
Indian	0.99	1.02	0.60	8.33	1273	300	13.3	1273	300

4. O_2 Reactivity Model Development, Results, and Discussion

4.1. Parent Model

Several authors[28, 37, 45] have also produced advanced annealing models. It is not necessary to thoroughly examine each of these models, but their common features are of interest. First, these models all used some form of distributed activation energy. In general, thermal annealing is the collection of processes that spontaneously occur to reduce the reactivity of a highly reactive raw coal particle to a relatively inert char particle, and all annealing processes are moving towards the thermodynamic minimum of a perfect carbon crystal. The wide range of annealing processes implies a distribution of activation energies, which suggests in turn that different portions of an activation energy distribution will be highlighted by experiments in different temperature ranges. That is, at a given temperature, some reactions will occur instantaneously (those at the low end of the distribution), but reactions with the highest activation energies are immeasurably slow. Only a subsection of the distribution of reactions will proceed on a time scale similar to the experiment, and so data over a range of conditions are necessary for a detailed characterization of the annealing activation energy distribution.[8, 46, 47]

Unfortunately, no single activation energy distribution form is uniformly accepted, but the log-normal and gamma distributions are both used in various models.[28, 37, 45] These distributions include very small activation energies that could result in considerable activity loss even at room temperature. Obviously, these low activation energy processes are not observed, and the distribution may be truncated to avoid them. Additionally, some deactivation processes that do occur at lower temperature would be essentially complete before any practical conversion

temperature could be reached. These processes could be included as part of the truncation of the energy distribution in the absence of adequate low-temperature annealing data. Finally, reactivity loss in these annealing models must be modeled on a relative basis, because the combustion reactivity of raw coal at 300 K is indeterminate (i.e., if the temperature is sufficiently elevated for appreciable oxidation rates, annealing is already well advanced). Since measuring the reaction rate of raw coal is not possible, the absolute loss of reactivity in the annealed coal is unknown. Together, these difficulties require that the annealing model be used in conjunction with an appropriate initial value of the preexponential factor for the heterogeneous reaction rate (where appropriate in this case means self-consistent with reactivity data and the annealing model parameters). A submodel should be included to predict the nominal A_o (the preexponential factor for conversion of raw coal) as in Hurt et al.[28] This requires some explanation, and since the annealing model developed below is a direct extension from the model of Hurt et al.,[28] Hurt's model is explored in greater detail. The assumptions in Hurt's model are:

- The annealing model is valid only with the associated preexponential factor submodel, and obviates the need for a truncated distribution. The submodel provides A_o, which is then reduced according to a time-temperature profile by the annealing model.
- The model has the potential to capture both physical and chemical effects, but was calibrated with annealing data obtained from inert environments. This assumes that an oxidizing environment would have minimal impact on the annealing process, which is likely a valid assumption in practical combustion cases because the high heating rate causes rapid devolatilization and initially prevents O_2 from reaching the surface.

- All types of active sites have the same *oxidation* kinetics. Available data necessitate this assumption, but, given the heterogeneous chemistry of coal, it is likely incorrect. However, each active site is assigned a different *annealing* (not oxidation) activation energy from the distribution.
- All sites have the same *annealing* preexponential factor.
- Annealing impacts the oxidation preexponential factor *only*. This assumption is not accurate, but it may be reasonable in typical air-fired combustion conditions.
- All reactivity data are assumed to be measured in zone I. This assumption obviously requires some care in data selection.

In the Hurt model, the deactivation model includes a preexponential factor and a lognormal distribution of activation energies. The lognormal distribution is fully defined by a mean and a standard deviation. The values of all parameters were determined by fitting the data, but the parameters were found to occupy a broad parameter space with no clear, uniquely optimal solution. These parameters are constant for all char and all preparation conditions, though Hurt et al.[28] observed that the assumption of constant parameters is not entirely valid.

From the observations and assumptions above, Hurt et al.[28] surmised that an appropriate oxidation preexponential factor model could have the functional form of Equation 1. They dealt with the precursor dependence as a separate correlation (Equation 2), which left the annealing model as a function of the time-temperature profile only. The annealing model functional dependence was determined by apportioning the total (unknown) number of active sites N_0 in "i" bins each with a unique activation energy, where relative bin size was determined by the

lognormal distribution. The annealing model then reduces to a series of i first order kinetic expressions, where N_i is the number of active sites in bin i, A_d is the preexponential factor of the annealing reaction, and $E_{d,i}$ is the annealing activation energy associated with bin i as seen in Equation 3.

$$A_{ox} = \mathrm{f}[precursor, T(t)] \quad (1)$$

$$\ln(A_0) = 10.96 - 0.07136 * \mathrm{C} \quad (2)$$

$$\frac{dN_i}{dt} = -A_d \exp\left(-E_{d,i}/\left(RT_p\right)\right) N_i \quad (3)$$

Again, the actual value of N_i is unknown (i.e., there is no way to count the number of actual active sites), so N_i is normalized by N_0. The model output is the ratio of the number of active sites remaining to the initial number of active sites, N_A/N_0=f[T(t)], where the ratio is known to initially be unity. Experimentally, this requires at least two reactivity data points to compare model output as a ratio of the two experimental measurements, which cancels the unknown N_0 from the equation and allows the model parameters to be fit to data.

N_i/N_0 initially follows a log normal distribution as in Equation 4. In Equation 4, $\ln(E_d)$ is considered as a variable rather than E_d, and thus the normal distribution of $\ln(E_d)$, yields a log normal distribution of E_d, where μ_{Ed} and σ_{Ed} are, respectively, the mean and standard deviation of the distribution. For any given value of activation energy for bin i ($E_{d,i}$), Equation 5 yields the ratio N_i/N_0 at t=0. Equation 6 is a discretized approximation for $i<\infty$, and holds at t=0, but as time proceeds, the series of i ODEs (Equation 7, where $f_i=N_i/N_0$) reduces the value f_i, so the distribution of active sites degrades to some irregular distribution. The sum of f_i at any time t>0

is some value less than unity, and, at fully kinetically-limited conditions, is directly proportional to the relative reactivity of the partially annealed char at a given time t.

$$N\left(\ln(E_d)\,;\mu_{E_d},\sigma_{E_d}\right) = \frac{1}{\sigma_{E_d}\sqrt{2\pi}}\exp\left[-\frac{\left(\ln(E_d)-\mu_{E_d}\right)^2}{2{\sigma_{E_d}}^2}\right] \tag{4}$$

$$\frac{N_i(E_{d,i})}{N_0} = \frac{1}{\sigma_{E_d}\sqrt{2\pi}}\exp\left[-\frac{\left(\ln\left(E_{d,i}\right)-\mu_{E_d}\right)^2}{2{\sigma_{E_d}}^2}\right] \tag{5}$$

$$\sum_i \Delta E_d \left[\frac{N_i}{N_0}\right]_{initial} = \sim 1 \tag{6}$$

$$\frac{df_i}{dt} = -A_d \exp\left(-E_{d,i}/\left(RT_p\right)\right) f_i \tag{7}$$

4.2. Conceptual Development

Considering the aggregate picture presented in the literature, and the experimental data, it is clear that coal annealing depends heavily on the precursor, heating rate, treatment time, and peak temperature. The literature also clearly highlights several of the most prominent thermal deactivation processes (loss of heteroatoms, carbon structure reordering, ash fusion etc.). Such diverse physical and chemical changes cannot be adequately captured by a single activation energy, at least not for a broad array of preparation conditions and precursors. Unfortunately, neither data nor computational power are available in sufficient quantity to rigorously model the vast diversity of annealing processes, so a distributed activation energy extended from the prior CBK model by Hurt et al.[28] is used. The literature observations in section 2 also imply that an

annealing model should only affect the preexponential factor in combustion kinetics, and is ambivalent on the subject of reactivity loss of O_2 vs. CO_2. Thus, the addition of an identical annealing model is possibly necessary to capture CO_2 activity loss (with appropriate parameter values tuned to CO_2 data). While, the CBK annealing submodel is an excellent starting point, it lacks a more subtle point found in recent literature observations. The annealing model as a whole depends on time, peak temperature, and heating rate, with the expectation that precursor differences fall under the purview of an additional submodel, while the actual distribution of activation energies is fixed for all coals and preparation conditions. Both the annealing literature and a basic understanding of coal combustion indicate that this is an oversimplification. The activation energy distribution simply states the relative abundance of various deactivation pathways. The following examples briefly describe why this distribution depends heavily on precursor and preparation conditions:

- In the case of the precursor, coals have widely varying chemical structures, sometimes even when their elemental composition is nearly identical. This variation can be observed not only between different coal seams, but also within the same seam to some degree. A different chemical structure implies a different distribution of annealing pathways.
- In the case of peak temperature, consider a coal with high catalytic ash content. This ash may limit pyrolysis or encourage graphite crystal growth by catalyzing crosslinking or carbon crystal rearrangement.[21-24] In such a case, the ash will fuse, eliminating the catalyzed deactivation pathway, if and only if a sufficient peak temperature is attained. A catalyst is defined, in part, by lowering the activation energy of a reaction pathway, so a

loss of a catalyst certainly changes the correct form of the distribution of annealing activation energies.

- In the case of heating rate, the importance of initial heating rate on pyrolysis is well established. As the extent of pyrolysis shifts for various heating rates, the chemistry of the newly formed char necessarily adjusts as well. Again, different char chemistry unavoidably leads to a different activation energy distribution.

Since annealing depends on so many variables, the lognormal activation energy employed in CBK and its many successors is intrinsically flawed. This lack of generality was unavoidable given the data available to Hurt et al.,[28] and while significantly more relevant data are now available, the data are far from sufficient to construct a perfect annealing model. However, given the arguments of more recent literature and data, it is possible to extend the CBK annealing model to include the effects of coal type, heating rate, and peak temperature. As in the Hurt annealing model, Equation 4 represents the log-normal distribution of the activation energy, which is divided into i "bins" with i activation energies (i=100 was found to be adequate). N_i, N_o, and f_i are also computed as discussed previously and shown in Equations 5-7.

Equation 7 is integrated over a time-temperature profile to arrive at a fraction of remaining reactivity, rather than an actual value for post-annealing reactivity. This is because the initial reactivity and N_o are not obtainable experimentally. In contrast to the CBK annealing model, the mean and standard deviation of the activation energy used here, along with the preexponential factor (Equations 8-10) become functions of coal type, heating rate (HR), and peak temperature experienced during heat treatment (T_{peak}).

$$\mu_{E_d} = \mathrm{f}(T_p, \text{Precursor, HR, reactive gas}) \quad (8)$$

$$\sigma_{E_d} = \mathrm{f}\left(T_p, p_0, \text{HR, reactive gas}\right) \quad (9)$$

$$A_d = \mathrm{f}\left(T_p, p_0, \text{HR, reactive gas}\right) \quad (10)$$

In the equations above, p_0 represents a coal-type effect based on chemical structure. While p_0 ranges only between 0 and unity, the majority of coals fall in a range with roughly 30% variation (see Figure 1); the model form uses scaled parameters so that the 0-1 range of p_0 is not overwhelmed by the ~1000-2000 K range that influences the T_{peak} parameter.

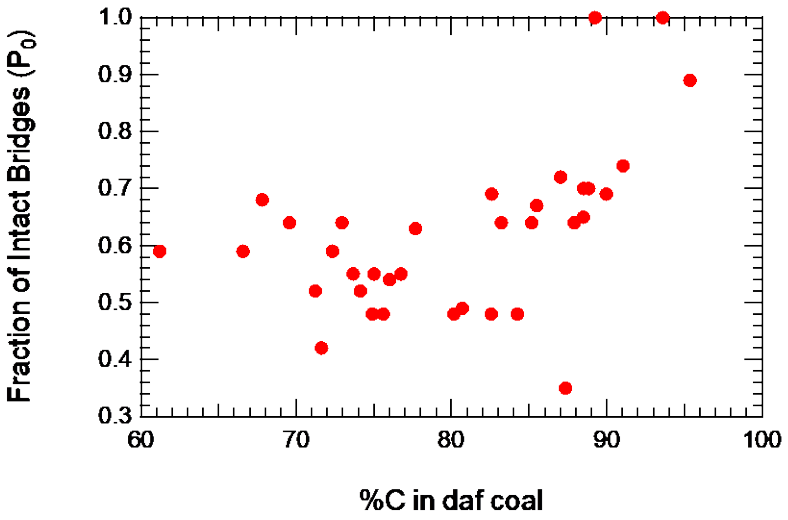

Figure 1. Measured values of p_0 for a variety of coals (from Genetti et al.[35]).

4.3. Model Calibration and Optimization

Having arrived at a theoretical dependency for an extended annealing model, finding the functional form relies on a statistical calibration tool, insight from past annealing experiments, a good deal of trial and error, and an optimization routine. The statistical calibration tool is complex, and numerous publications have been devoted to various iterations, applications, and

development of the method. This method is explained only in the briefest, most conceptual manner here, with further details available elsewhere.[48-51] The calibration can be broken into six steps, as demonstrated in Figure 2.

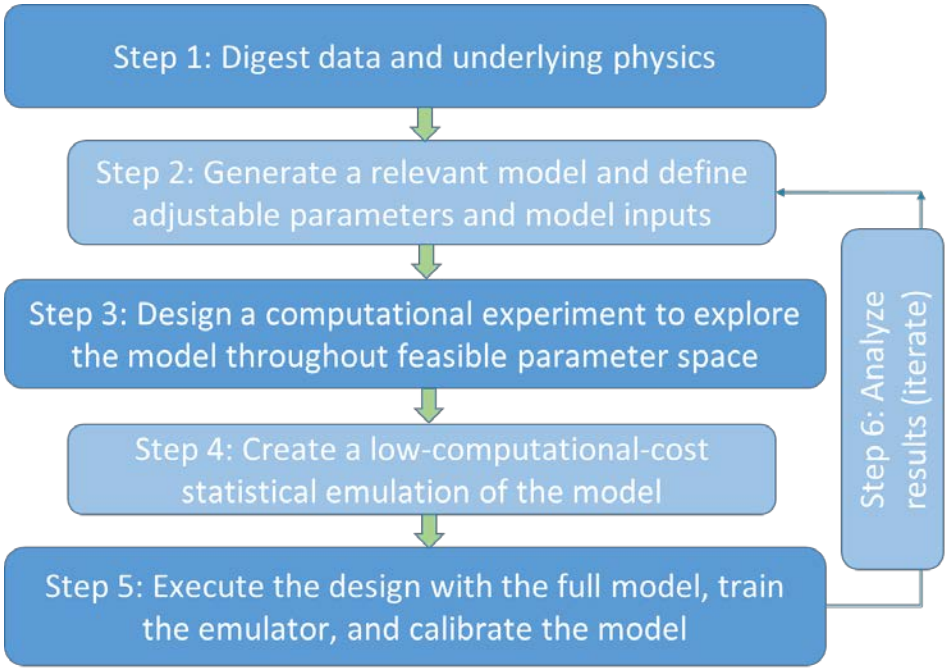

Figure 2. Logic map of the model calibration process

The first two steps consist of understanding the physical phenomena in question and coding a relevant model. Step 1 simply involves building a physical intuition that allows the investigator to create a reasonable model and produce well-founded expectations for how the model will behave, and how model parameters are interrelated. Step 2 is often an Edisonian attempt to capture observations in an acceptably simple model, guided by the intuition developed in step 1. The latter four steps require an extended explanation, given in the following four subsections. These steps are experimental design (for a computational experiment), model emulation, model

calibration, and model results analysis. Note that Equation 11 shows a generic model form for Bayesian statistical calibration.

$$y_i = \eta(\mathbf{x_i}, \boldsymbol{\theta}) + \delta(\mathbf{x_i}) + \varepsilon_i \quad (11)$$

In Equation 11, η is a model that depends on both experimental inputs and model parameters (typically, η is the statistical emulation of the model designed in step 2). Similarly, δ is a function that reflects the discrepancy between model and reality (i.e. it tracks errors introduced by imperfect assumptions), and ε is the noise observed in experimental data.

4.3.1. Computational Experimental Design

In designing a computational experiment, the first step was to determine model input and parameter ranges. In Equation 11, y is the model output (where the model output is the sum model predictions (η), model discrepancy from reality (δ), and observational error (ε)). Equation 11 has a vector of model inputs (**x**), and a vector of model parameters (**θ**). In the case of the original annealing model, **x** values were restricted to a time-temperature profile, and **θ** values were limited to the mean and standard deviation of the activation energy distribution and the annealing preexponential value. The range of permissible values for each experimental input and model parameter was used to set up a Latin hypercube[52] sampling scheme. The hypercube accepts as inputs the allowed range and probability distribution of each parameter. The range is then divided into a specified number of equiprobable intervals, and one parameter value is chosen at random from each interval. For example, if 10 runs were desirable, the parameter space would be divided into 10 intervals. In the case of a uniform probability distribution, each of the 10 intervals would be of equal "length" in parameter space, while in the case of a normal

distribution on the parameter space, the intervals near the mean parameter value would be much "shorter" than the intervals in the tail. Because each interval contributes exactly one parameter value, most of the samples would cluster around the mean, and the low probability sample space would not be well explored. The sampling process is executed for each parameter and input (**θ** and **x**), and the values are then systematically paired to be optimally space filling.[52] The result is a matrix in which each column "j" contains randomly ordered, unbiased, space-filling samples from the range of parameter (or input) "j", and each row "i" is a set of all necessary input values and model parameters for a single computational experiment. In other words, each row of the matrix constructs a time-temperature profile and designates a value for the mean, variance, and preexponential factor of the annealing activation energy. The number of columns equals the number of parameters plus the number of inputs, and the number of rows is the number of computational experiments to be performed.

4.3.2. Statistical Model Emulation

The calibration procedure requires exploration of model behavior throughout the allowable ranges of inputs and parameters. This allows the calibration machinery to reject unsuitable parameter space by assigning a low probability to poorly performing regions of the sampled space. However, numerous executions of the model are required, and most computational models incur a non-trivial computational cost in the case of even moderately high-dimensional parameter spaces. Here, model execution costs may be as low as fractions of a second and still be considered non-trivial, depending on available computation resources, so models that require weeks or months are certainly not feasible. This difficulty is circumvented by implementing a

statistical emulator, trained by the results of the computational experiment designed in the previous section. An emulator accepts any set of inputs and parameters, and produces outputs that approximate the full model. The emulator result is computed very quickly, and includes an estimate of output uncertainty. The full annealing model was executed with 400 sets of inputs and parameters from the Latin hypercube design discussed above, and the corresponding inputs and outputs were used to train a Gaussian process emulator, as described in detail elsewhere.[48-50] In essence, the Gaussian process is a multivariate normal distribution fully defined by a vector of mean values and a covariance matrix. In principle, the values of the mean and covariance are trained to model outputs such that the Gaussian process can predict the model output for any given set of inputs and model parameters. In practice, this may be only partially successful due to poor mathematical behavior in the model. Such problematic cases include, for example, a model where large, irregular shifts in output correspond to small adjustments in the inputs, or due to a poorly explored model parameter space. The model emulator is represented in Equation 11 as $\eta(\mathbf{x}_i,\boldsymbol{\theta})$, while the other two terms (δ and ε) are additional Gaussian processes.

4.3.3. Model Calibration

The terms ε_i and $\delta(\mathbf{x}_i)$ represent the model discrepancy and experimental error, respectively. The experimental error is a collection term for observational error, variation between experiments, potential experimental bias, etc., and is used to quantify the uncertainty inherent in the experimental data. In annealing experiments, this uncertainty is relatively large. The discrepancy term quantifies the ways in which the model fails to match reality, even after all sources of experimental error are taken into account. This term enhances the model calibration process by

analyzing the difference between the model predictions and experiment, and describing where the model fails, to what degree, and with respect to which inputs.

This may be illustrated with the well-known model for ballistic motion in Equation 12, which is derived by integrating the acceleration due to gravity twice with respect to time.

$$x(t) = \frac{1}{2}gt^2 + c_1 t + c_2 \tag{12}$$

Here c_1 and c_2 are the constants of integration and represent initial velocity and position, respectively. Assuming c_1 and c_2 are both zero, the model reduces to $x(t)=g/2*t^2$, and perfectly captures the position of a falling object in a vacuum. If such a model were to be calibrated, experimental observations would be imprecise, leading to a non-zero ε_i. Additionally, if the experiments did not take place in a vacuum, the results would become increasingly erroneous as the drag force increases, but is not accounted for. This discrepancy between model and reality would be revealed and attributed to the input, (i.e., time). This is because the lack of drag force induces no error at t=0. Instead the error is observed when velocity is non-zero, and is exacerbated as velocity increases with time. The low dimensionality of this trivial example is amenable to graphical inspection. Simply plotting the calibrated model predictions with the data (both with respect to time) would show model discrepancy as t increased. Model discrepancy in the case of the falling object also lends itself well to diagnosis via physical intuition, in that drag force is a daily experience that can easily be conceptualized. In fact, it is counterintuitive that a feather and a bowling ball fall at the same velocity in a vacuum, because daily experience is not a vacuum. Similarly, physical phenomena models beyond the range of direct human experience are often counterintuitive, and thus difficult to visualize and diagnose, especially when they

incorporate a high-dimensional parameter space. Such models benefit from a quantified model misfit with respect to parameters and inputs.

4.3.4. Calibration Results and Analysis

In the interest of brevity, the details of the statistical analysis are not given. To summarize, the analysis found the CBK annealing model to be overwhelmingly uncertain, which is in fact consistent with the statement by Hurt et al.[28] in the publication of the original annealing model. The model uncertainty was substantially reduced by applying a greater wealth of data, a better exploration of parameter space, and a coal structural parameter as a dummy input, but considerable uncertainty remained. The dummy parameter had no impact on the model whatsoever, but it did allow the statistical machinery to attach a discrepancy to the input, and indicate the level of functional dependence an annealing model *should* have. The subsequent analysis indicated that the time-temperature profile and the coal structural parameter were by far the largest sources of discrepancy between the model and the data. This was quantified in an internal statistical parameter for the covariance matrix of the discrepancy (δ) term. The covariance parameter necessary to capture the discrepancy due to precursor structure and the time-temperature profile were each about a factor of five greater than discrepancy in other parameters.

The insights from the statistical calibration tools and the observations of the literature led to a campaign of informed trial and error to uncover the model functional form (step 6 in Figure 2); this ultimately reduced the model uncertainty and average prediction error substantially. The extended annealing model is executed precisely as the prior CBK annealing model, with all

changes successfully confined to the annealing activation energy distribution and the annealing preexponential factor. The model was inspired by literature implications for functional dependence on heating rate, T_{peak}, and the precursor chemical structure, but balanced with a need to minimize the total number of parameters that would effectively be relegated to fudge factors in an over-parameterized optimization. Note however, that despite considerable model improvement, annealing is still an umbrella term for numerous processes that include enormous variability. The current model performs well, given the current data, but substantial improvements could be made by both specifying which processes should fall under the auspices of annealing, and conducting sharply focused research on the specified processes.

Equations 13-17 describe the final functional form of the preexponential parameter for annealing (A_d), the mean annealing activation energy (μ_{Ed}), and the standard deviation for the annealing activation energy distribution (σ_{Ed}) (see Table 5 for parameter values). Note that the model inputs are p_0, HR, and T_p. The values of HR and T_p are given in K/s and K, respectively, but the actual inputs are divided by their native units so that all inputs are unitless. The input p_0 is naturally unitless, and the parameters have the units of $\ln(\mu_{Ed})$ (i.e., ln(kcal/mol)).

$$if\ HR < 10^4 \qquad A_d = \frac{p_0 * A_{d,0}}{\ln(HR + 2.7)} \tag{13}$$

$$if\ HR \geq 10^4 \qquad A_d = \frac{p_0 * A_{d,0}}{\ln(10^4)} \tag{14}$$

$$if\ T_p \leq 1500 \qquad \ln(\mu_{E_d}) = \mathrm{a} * p_0 + \mathrm{b} + T_p * c/1000 \tag{15}$$

$$if\ T_p > 1500 \qquad \ln(\mu_{E_d}) = \mathrm{a} * p_0 + b \tag{16}$$

$$\ln(\sigma_{E_d}) = \frac{\ln(\sigma_0)}{p_0} \tag{17}$$

Equations 13 and 14 express the heating rate dependence on the original number of active sites. Cai et al.[19] found that higher heating rates increased the reactivity of a char considerably with all other preparations conditions held constant. The natural log of the heating rate captured the reactivity increase well up to about 10^4 K/s, after which a plateau was reached for all coals tested. The increase in activity is speculatively attributed to an increase in micropores during increasingly rapid devolatilization. This implies that the annealing model is perhaps not the ideal submodel to include this information, but in general, comprehensive char combustion codes do not include a submodel to address preparation condition-based pore development. Therefore, the umbrella of annealing with built-in preparation condition dependence is the most appropriate submodel available. Any model employing an estimate of porosity based on heating rate would be well served to eliminate the heating rate dependence of the annealing preexponential factor. Note that the heating rate dependence is located in the denominator because A_d describes how rapidly annealing proceeds. If the surface area increases by some factor "F", the number of active sites is expected to increase by the same factor "F" (assuming uniform active site density). This is captured in the annealing submodel by reducing the rate of site destruction by "F," where F=ln(HR+2.7) (note that F reduces to ~1 at very low heating rates). This is not mathematically identical to increasing the number of sites by "F," but the number of active sites was normalized to unity as is appropriate for a lognormal probability density function, and it is undesirable to disrupt the normalization. Since the annealing model is far from mathematically perfect in any case, it was deemed conceptually adequate to adjust the preexponential factor to decrease the rate

of reactivity loss instead. Finally, the structural parameter p_0 is included, where p_0 specifies the fraction of intact bridges in the coal pseudo-monomer. The intact bridge fraction is experimentally found via NMR spectroscopy, or derived from a correlation via the proximate and ultimate analysis as described by Genetti et al.[35, 53] There are four NMR parameters commonly used to describe coal structure, all of which appear strongly correlated with each other and were found to be equally suitable for a coal structural parameter. The NMR parameter p_0 was chosen to represent coal structure after only moderate success with the simple ratio of carbon to hydrogen from the ultimate analyses. The C/H ratio does not distinguish between radically different coal structures with a similar elemental composition, but the NMR structural parameter approach has been successfully employed elsewhere [54, 55].

Equations 15 and 16 are a straightforward linear model to predict the mean (μ_{E_d}) of the log-normal activation energy distribution, given coal structure and peak temperature, with the addition of some constant, "b." The only subtlety is that the peak temperature dependence may be profitably turned off at peak temperatures above 1500 K, where the literature indicates many T_{peak} effects were no longer relevant. In fact, a series of models that employed the T_{peak} term *above* 1500 K (and turned off "c" *below* 1500 K) found that the optimal value of "c" was driven towards zero (i.e., T_{peak} is not an important parameter input for the mean activation energy above 1500 K). Equation 17 predicts the standard deviation of the distribution, and, together with Equations 15 and 16, fully defines the log-normal activation energy distribution. The model standard deviation was found to be relatively constant with respect to T_{peak} and heating rate, with a direct dependence on char precursor. The functional dependence of σ_{EA} on precursor only is reasonable as a given coal should have some distribution of activation energies, but T_{peak} and HR

likely shift the center of that distribution more than they adjust the range. Once μ_{Ed} and σ_{Ed} are defined, the log-normal distribution is known. After the log normal distribution is defined, it is split into a bimodal distribution in accordance with numerous observations of two distinct annealing regimes in the literature.[36, 56, 57] This is done by the factors B_f and B_r, which are both optimized values, so the actual location of the bimodal trough is also determined by optimization. The factors B_f and B_r split the log normal distribution by isolating the activation energies in the range: $\mu_{Ed} - B_f < \mu_{Ed} < B_f + \mu_{Ed}$. The density of active sites within that range is divided by B_r. In other words, B_f indicates the breadth of a trough in the bimodal distribution (centered on the mean), and B_r determines the depth of the trough. The formerly log-normal distribution is then renormalized, which maintains the total number of initial active sites, but allows for a bimodal distribution with an optimized weight between the two regimes.*

Figure 3 below is a sample log normal distribution that shows the fraction of active sites in any given bin. The exact mean and variance of the distribution depends on heating rate, precursor NMR parameters, and peak temperature. Figure 4 shows an irregular, bimodal distribution after parameters B_r and B_f are applied and the distribution is renormalized. The second figure has two striking features. First, the majority of the low activation energy sites vanish. This is not a problem in either of the two distributions, because the original log normal distribution resulted in a highly exaggerated rate of initial annealing, which was compensated for by using an

* The bimodal distribution factors B_f and B_r are a complex series of operations as shown in the script "match_reactivity" found at https://github.com/tmholland86/CCK-oxy (LA-UR-17-24629).

excessively high initial preexponential value. The reduced initial annealing of the second figure dispenses with the need for an excessively high initial preexponential factor. The second notable feature is that the second peak of the distribution is highly irregular. This indicates that, after the very rapid initial annealing, the remaining activated annealing processes have a large number of active sites at a high activation energy, so the remaining annealing processes will be relatively gradual.

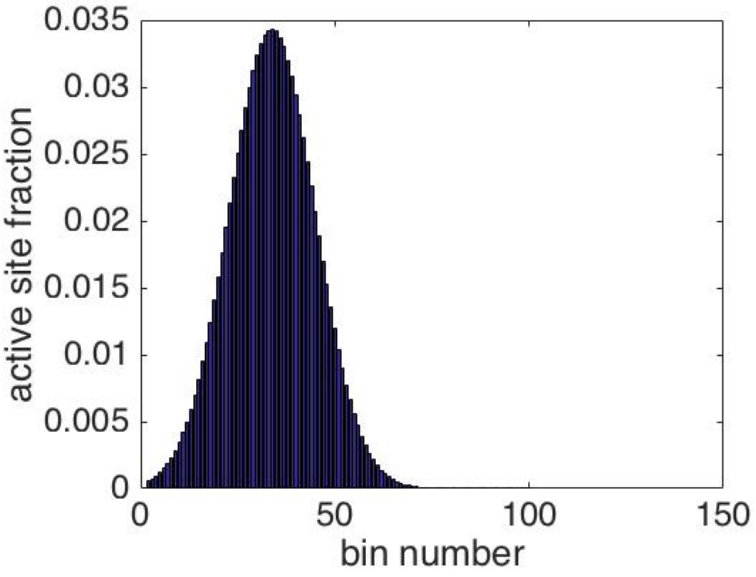

Figure 3. Sample log normal distribution of the fraction of active sites in any given bin.

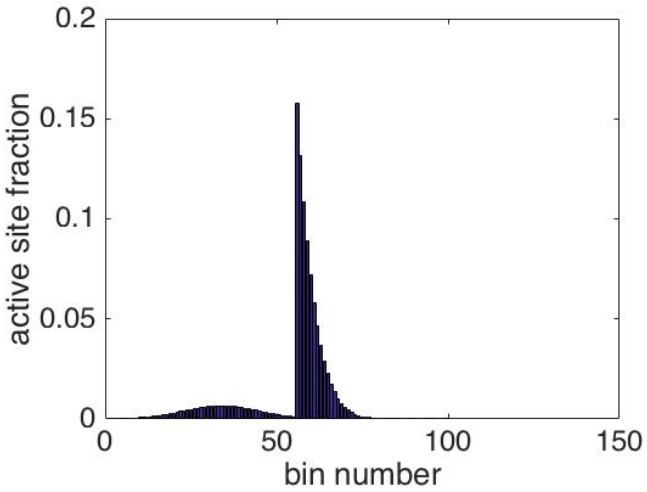

Figure 4. Sample "bimodal" distribution after applying the parameters B_r and B_f and renormalizing the distribution.

4.4. Model Optimization

Once a reasonable model form was developed, the model parameters were optimized. The optimization routine was coded using fmincon in MATLAB, which traversed the bounded parameter space of the model in an attempt to minimize an objective function. Thus, the annealing data are not fit via a standard linear regression. In fact, the model parameters cannot be directly regressed because even the conceptual form of the model is far from linear in its parameters, and even if the model could be linearized, such a mathematical transform would render a regression statistically invalid. Instead, the optimization routine finds a narrow subsection of parameter space containing numerous local minima, many of which lead to approximately the same model output. Any vector of parameter spaces that leads to a reasonable local minimum is valid, and finding the absolute minimum in a high dimensional, non-linear parameter space is essentially impossible. Instead, the optimization is carried out by implementing various parameter bounds and constraints, and initializing the optimization from

different locations in parameter space. Each optimization required roughly 12 hours on a 2016 MacBook Air, and, after dozens of optimizations, approximately 1/3 failed (settled on a local minimum that was clearly far from the global minimum) and 2/3 succeeded (located local minima that were all roughly equal, and presumed to be near the global minimum). Table 5 gives the values of the annealing model parameters used in the results section. The optimization routine yields a single local minimum. In producing Table 5, the optimization routine was executed numerous times with different initial values in the parameter space, and in about half of all cases a local minimum in the objective function was found within 5% of the objective function value produced by the parameters in Table 5. In almost all other cases, the objective value was within 50% of the superior local minima, and there were a handful of optimization failures. The particular values in Table 5 were chosen because they were the lowest found, but in this model there are numerous essentially equivalent local minima, and an infinite number of surrounding points in parameter space that are equivalent for any practical purpose. Note that the parameters a and b are on similar scales, while c (relating to the influence of peak particle temperature) is roughly an order of magnitude smaller. Since the temperature and NMR parameters were scaled to be similar, this indicates the relatively low impact of peak particle temperature, which is expected, since most of the available data are at relatively high temperature.

Table 5. Annealing model parameter values.

Parameter	Value	Units
$A_{d,0}$	9.71×10^{11}	s^{-1}
B_f	45.55	kcal/mol
B_r	176.66	-

a	0.46	ln(kcal/mol)
b	1.77	ln(kcal/mol)
c	7.32×10^{-2}	ln(kcal/mol)/K
$\ln(\sigma_o)$	0.65	ln(kcal/mol)

5. Model Execution Results and Discussion

The final annealing model predicts the relative reactivity of a char compared to some reference char, as discussed previously. This is because reactivity is measured directly, but the number of active sites (either initial or final) cannot be measured. Instead, by taking the ratio of reactivity in two annealed chars in a zone 1 combustion regime, the ratio of final active sites can be determined (relative to the initial active sites). Therefore, each set of annealing data has a single char designated as a reference, and the data points are the ratio of the reactivity between each char and the designated reference char. The annealing model is considered to be performing well when the measured relative reactivity is close to the predicted relative reactivity. Because the model parameters were optimized, an objective function was required to quantify "close." Because the annealing data covered a very wide range of coals and conditions, the results cannot be conveniently displayed in a meaningful way. Simply plotting the measured and predicted reactivities on the ordinate axis (with an index on the abscissa) resulted in an unreadable mess due to the variation in scale between experiments. Ultimately, it was decided that several measures of model success should be included. A log-scale parity plot is shown in Figure 5 partially to show all of the O_2 data in one compact location, and partially because the original CBK annealing model results were displayed on a log parity plot. A linear parity plot has the dual difficulties of requiring a very large axis to display the outlier points from the Hurt model,

while simultaneously compressing the majority of the points into a tight region not amenable to visual inspection. The log-scale plot on the other hand, can be quite misleading and give the impression that the extended annealing model developed in the present work is only a minor improvement over the prior model. Note that, in accordance with the discussion in the model development section, the **relative** reactivity is used in Figure 5 because the actual degree of activity loss can only be observed as a ratio between two chars that received different heat treatments. Thus, every data set includes a reference char with a measured reactivity, and the ratio of reactivities between the reference char and any other char in the data set is the (unitless) relative reactivity. Note that the choice of different reference char does NOT impact the results of the model or calibration, but it does change which side of the parity plot (over or under prediction of relative reactivity) that any given data point falls.

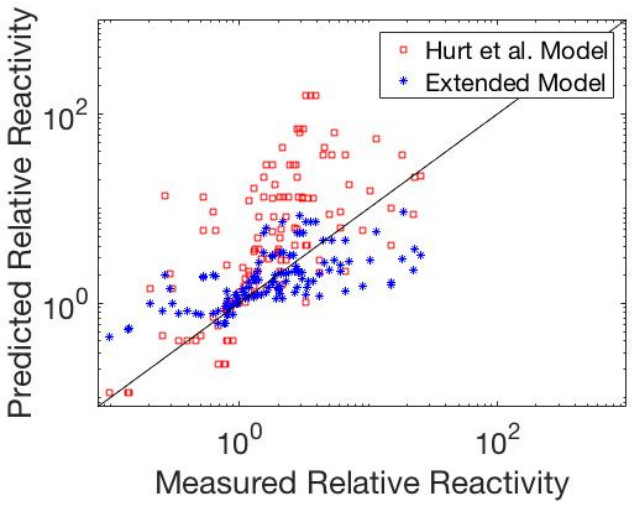

Figure 5. Parity plot of measured and predicted relative reactivities in O_2 for the Hurt et al.[28] mod vs the extended annealing model

In contrast, Table 6 includes the results of the sum-squared error as an equally misleading measure. Superficially, the sum-squared error indicates that the extended model is ~2 orders of magnitude superior to the prior model, but in reality a relatively small handful of points result in enormous error. The best measure of model success, both for an optimization objective function and for reasonable model comparison, is referred to in Table 6 as the error factor (which is a quantity defined and described in detail in the experimental section). Table 6 includes the mean and range of the error factor for entire body of data as well as several subsets. This breakdown shows that the extended model is certainly an improvement, but the improvement is closer to a factor of four rather than a factor of 100. Additionally, the quartile breakdown shows that the extended model performs well across the board with only a small handful of egregious failures, while the CBK annealing model has numerous large errors in all but the best performing quartile. In other words, the prior (Hurt) annealing model is effectively either on or off, and accurate only in a small subset of conditions. Note that, while it would be desirable to compare the original CBK annealing model directly to the extended annealing model, the extended annealing model requires more detailed information that was not available in the referenced literature for the Hurt model, so direct comparison using the original subset of data from the Hurt model is impossible.

Table 6. Measures of Extended Model Success Compared with the Hurt et al.[28] model for the Entire Annealing Data Set

	Hurt et al. Model			Extended Model		
Model Quantification	**Mean**	**Minimum**	**Maximum**	**Mean**	**Minimum**	**Maximum**

Sum Squared Error	$1.45x10^{5\dagger}$	N/A	N/A	$2.43x10^{3\dagger}$	N/A	N/A
Error Factor: All Points	**6.08**	**1.00**	**51.97**	**2.24**	**1.00**	**9.96**
Error Factor: Least Successful Quartile	17.28	7.00	51.97	4.44	2.30	9.96
Error Factor: Most Successful quartile	1.13	1.00	1.25	1.10	1.00	1.20
Error Factor: Central Quartiles	2.78	1.25	6.50	1.63	1.21	2.27

On average, the extended annealing model predictions differ by a factor of about 2.24 from measured values. An average error of 124% is far from an optimal model, but in comparison to past work (with an average error of 508%), it is a significant improvement (a factor of ~4). It is worth noting that carbon sources are notorious for enormous variability in their respective reactivities. In fact, it seems likely that the umbrella of effects referred to as annealing are responsible for such a large range of reactivities. There are insufficient replicates in the data for a detailed statistical analyses of variance within individual data sets, but a brief examination of the few replicates or pseudo-replicate data points is enlightening. Among these data,[22, 58] the variation between replicates ranges from roughly 20-50%. Thus, 124% error is not at all

† This is a single value, not a mean of multiple values.

unreasonable, and is in fact a substantial stride towards mitigating the vast uncertainty of coal combustion rate modeling, perhaps even to the extent that a coal-general kinetic correlation may be feasible if derived in conjunction with a comprehensive char conversion model.

5.1. Model Predictivity

The present annealing model was developed with a minimal number of adjustable parameters specifically to avoid a large number of "fudge factors" that would fit virtually any data set while having very low predictive power. However, a model with few parameters is no guarantee of predictive power. As observed above, the annealing model employed in CBK and its successors often predicted annealing quite far from experimental data, probably because the model was calibrated using relatively few data points from a narrow selection of precursors and preparation conditions. Given that a substantial amount of uncertainty remains in the current annealing model, it was entirely possible that the new model would suffer from a similar handicap. Therefore, several data points were initially excluded from the optimization objective function to test the model predictivity. In general, the model predicted the new points with remarkable success, and when the model parameters were re-optimized with all data points, the new data had a minimal impact on the overall model calibration. One such data set is shown below in Figure 6 (data collected by Jayaraman et al.[44] for a high-ash Indian coal). The ordinate axis is the relative reactivity NOT the error factor. The error factor (calculated as described in Section 3) in this case ranged from 1.00-1.12, with a mean of 1.08. In general, any ratio less than ~2 is considered quite good in the context of reactivity loss. The abscissa is potentially misleading in that up to six input variables influence each data point (the heating rate, treatment time, and peak temperature

for the char particle, and the same three variables for the reference char). However, the peak temperature of the char particle is most likely to both change and have a dramatic impact between points, so it was deemed the best variable for the abscissa in the absence of six-dimensional plotting software. Nevertheless, the apparent replicates are not actually identical data points.

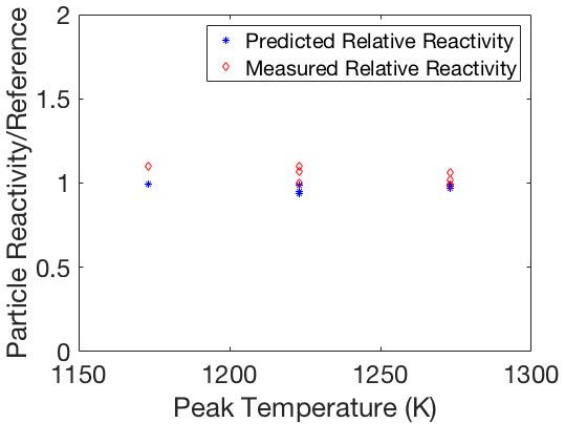

Figure 6. Model predictions compared to experimental measurements of an Indian coal (data were not used to calibrated model).

At first glance, Figure 6 can be misleading. It is natural to intuitively view the annealing values close to unity as uninformative. However, an annealing value near unity does NOT indicate a lack of annealing. Instead, it indicates that the annealing of the data point and the annealing of the reference char were very similar. The agreement in Figure 6 is therefore an exceptional example of model success in that it tracks annealing quite well even at conditions or treatment times that are very similar. The predictions and data are not identical, and the predictions have a

slight but consistent negative bias, which indicates that the annealing model is not exact, but it is correctly responding to subtle changes in heat treatment.

Additional comparisons of predictions and measured data (and associated error factors) are shown in Figure 7 and Table 7. In all cases, the ordinate axis is the relative reactivity NOT the error factor. The error factor mean and range are reported in Table 7. Figures 7a and b both show data from experiments with Pittsburgh 8 coal, but from two different investigators. Figures 7c through f show a variety of other coals over the range of experimental data. In general, the model predictions are quite good, with obvious outliers at the lowest heat treatment temperatures. The poor predictions at low temperature are much worse than the average predictions, and while the lack of agreement in this region is undesirable, it is not unexpected. The raw coal precursors are quite diverse, and low heat treatment temperatures do not allow the chars to progress as far towards the thermodynamic minimum of a perfect graphite crystal. Thus, the mildly annealed chars retain greater diversity. Also, low-temperature heat treatments likely do not fuse the ash. The chemical identity of the ash is rarely characterized in individual coals, so ash variation between char precursors is not reflected in the annealing model. This creates additional model uncertainty for low-temperature char preparation because ash has fusion-dependent chemical and physical effects on the coal. More importantly, the low-temperature heat-treatment implies a drastically different devolatilization process, which significantly alters the chemistry of the char. Ultimately, the low-temperature predictions are of far less practical importance, and are not cause for significant concern in practical char conversion models.

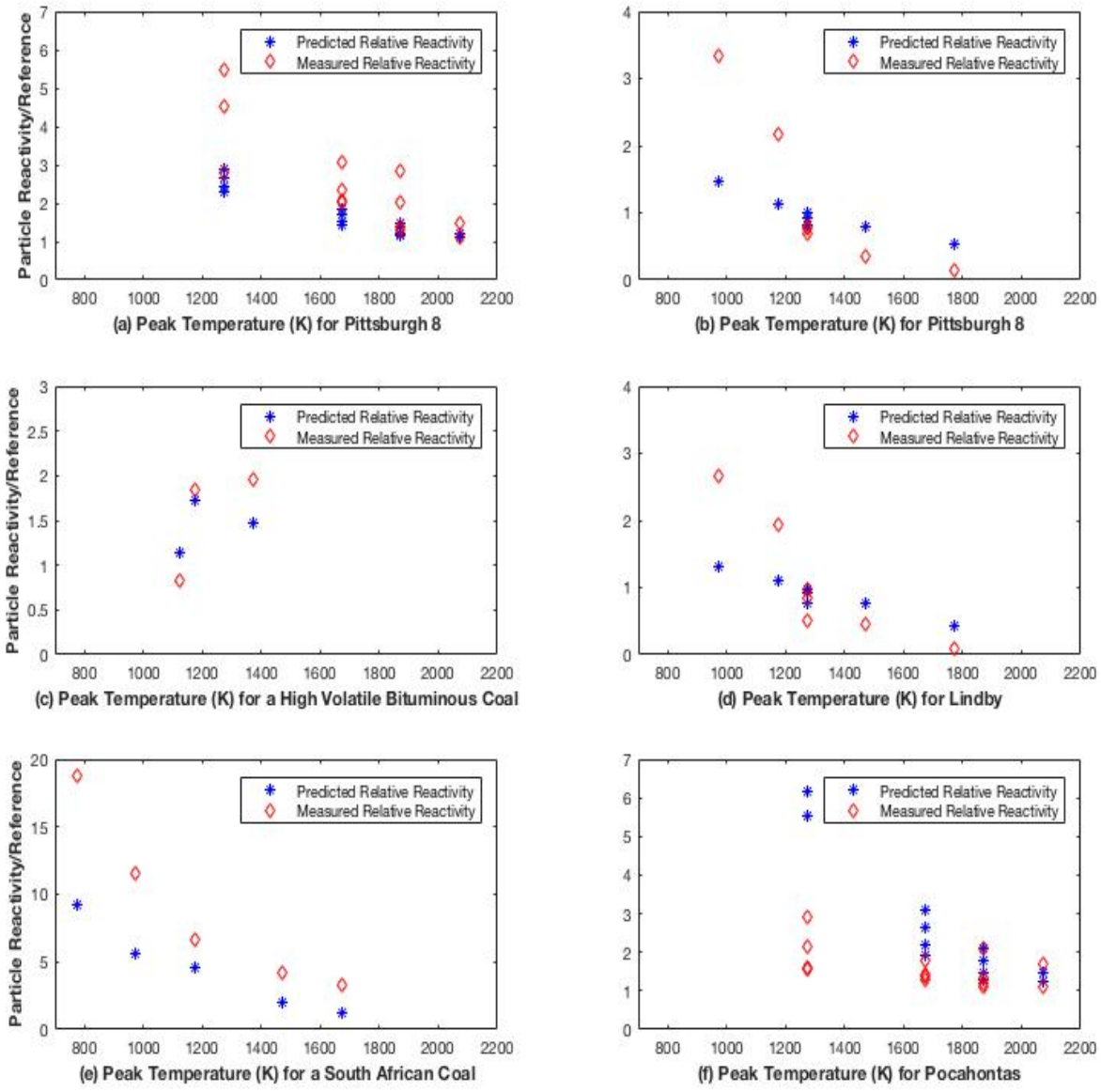

Figure 7. Diverse selection of char relative reactivities (both predicted and measured). See Table 7 Error! Reference source not found..

Table 7. Error Factors Associated with a Diverse Selection of Coals.

Coal	Min Error Factor	Max Error Factor	Mean Error Factor
Pittsburgh 8 [37]	1.01	1.92	1.41
Pittsburgh 8 [19]	1.20	3.84	2.00
HVB [39]	1.06	1.37	1.26
Lindby [19]	1.01	4.50	1.92
South African [38]	1.44	2.73	2.06
Pocahontas [37]	1.00	3.84	1.95

5.2. Model Failure

Despite the general success of the model in fitting data (and predicting data it had not yet been calibrated to), there were a number of significant model failures (5.1%), defined as model predictions greater than a factor of five from the experimental data. Among these failures, all but a single point of data had several commonalities. First, all of the data points in question came from two authors,[20, 40] and both of these authors formed their char in a flat-flame burner. The data sets from both authors appeared to have a very high variance, in that supposedly similar experiments led to widely different results without a definite trend; however, the actual variance cannot be computed, as replicates are not given. Third, both sets of experiments sampled data on a short time scale, and fourth, both authors obtained a number of points that agreed remarkably well with model predictions, both before and after the questionable data was included in the optimization routine. Finally, both data sets included coals that were used by other authors in annealing experiments, with vastly different results.

It is possible that the annealing model is simply unable to predict flat flame burner chars. However, given that many of the chars in the same data sets were predicted very accurately, it

seems far more likely that the short time scale and sampling limitations in the flat flame burner led to noisy data. A sample of the worst model failures and adjacent successes to supposedly similar experiments is given in Figure 8 (data from Shim and Hurt[20]).

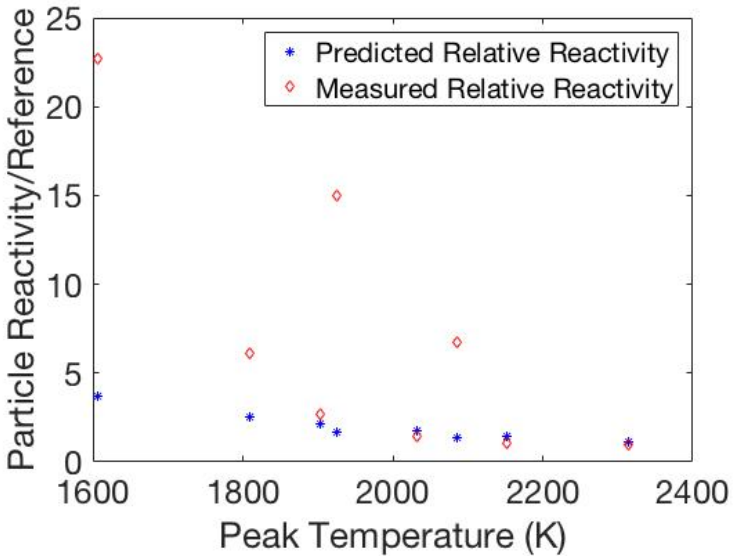

Figure 8. Model predictions of the Shim and Hurt data set, both failures and exceptional successes.

5.3. Sample Model Predictions

While the extended annealing model was broadly successful in predicting char reactivity loss due to preparation and combustion conditions, there was one large data set that consistently failed. The failure was not large in terms of error factor, as with the handful of anomalous, erratic points. Instead, it was a consistent failure to track a subtle trend in char reactivity with treatment time in a Chilean coal.[36] Figure 9 shows that the model does reasonably well predicting the degree of annealing in an absolute sense, but an additional dimension of treatment time shows that the model remains essentially constant with the very small changes in treatment time (shown by the vertical distribution of points at any temperature). This was ultimately determined to be

the reason that the statistical calibration tool found substantial model discrepancy with treatment time. Physically, it is caused by the approximation of the initial heating time-temperature profile. Because detailed data were not available to reasonably estimate the time-temperature profile, the initial heating rate was used as a crude substitute. In general, the estimate is sufficient, but when the heating time is a significant portion of the total annealing time, the error can become noticeable. This error was further verified by attempts to fit only the data in Figure 9 without any other experimental data, but the results were not improved, even when several different model functional forms were attempted. Also, when the data were excluded from the objective function, the annealing model predictions did not change notably (and still gave the reasonable predictions seen below). Conversely, when the data of Figure 9 were included with all other data, model predictions were also not significantly influenced; the extended annealing model simply cannot fit the subtle trend of a data set with very short treatment times in the absence of a more accurate heating profile.

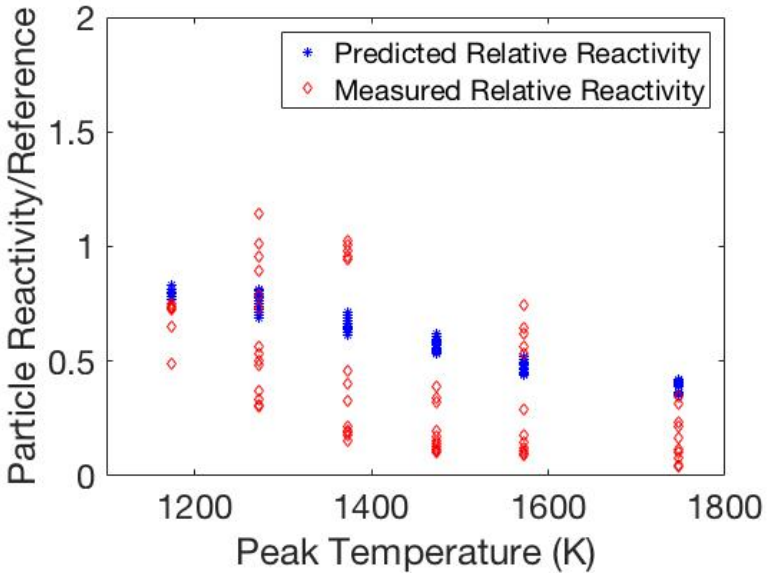

Figure 9. Model predictions and experimental data for Cerrejon coal.[36]

5.4. CO_2 Model Development and Results

The literature implied that activity loss to CO_2 gasification potentially proceeds along different kinetic pathways than O_2 annealing. By extension, steam reactivity reduction may also behave differently than combustion annealing. In general, CO_2 and steam may be neglected as reactants in pulverized coal combustion, but the extended annealing model is intended to function in an oxy-fuel setting as well, where CO_2 and H_2O may have appreciable influence on the combustion process. Therefore, it seemed prudent to tabulate CO_2 annealing data and attempt a similar calibration for an alternative annealing model form, or at least determine alternative parameter values if the same functional form turned out to be adequate. However, as a matter of curiosity, the O_2 calibrated annealing model was applied directly to the CO_2 and steam data, and in general performed astonishingly well considering the lack of calibration. It must be noted that there was relatively little CO_2 data available, and that one large set of data fit extremely well, forcing the

mean error factor down. However, the results in Table 8 and Figures 10-11 clearly show that, within the limits of available data, the model is able to predict CO_2 and H_2O annealing adequately even with the parameters calibrated to O_2 annealing. Figure 10 contains data for a South African Coal, which was also used in several of the O_2 data sets, although the CO_2 experiments were from a different lead author and institution.[38] This may well have improved the uncalibrated model prediction in the case of South African coal, but the uncalibrated model was also successful with other coals in the CO_2 environment. The same annealing model form and parameters therefore seem appropriate for both O_2 and CO_2 activity loss. Recall that Figure 10 shows the model predictions, not the error factor, so the model is actually performing even better than the plot implies. Figure 11 represents the sole H_2O data set available.[44] The small sample size limits inference, but the model appears to perform exceptionally well for H_2O annealing as well. Because the model form and parameters captured all available data well (O_2, CO_2, and H_2O reactivity) even when the model was calibrated to O_2 only, the final model and the values reported in Table 5 were calibrated using all available data in all conditions and reactive gases.

Table 8 – Uncalibrated CO_2 and H_2O extended model annealing predictions.

Model Quantification	Mean	Minimum	Maximum
Sum Squared Error	268*	N/A	N/A
Error Factor: All Points	1.66	1.00	4.96

* This is a single value, not a mean of multiple values.

Error Factor: Least Successful Quartile	2.84	2.05	4.96
Error Factor: Most Successful quartile	1.04	1.00	1.08
Error Factor: Central Quartiles	1.37	1.09	2.02

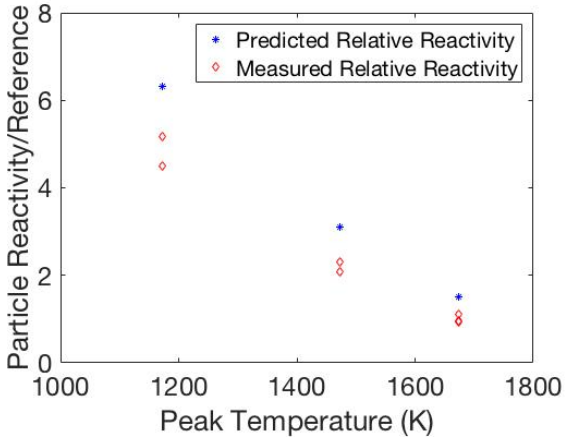

Figure 10. CO_2 Annealing data and uncalibrated model predictions for a South African coal.

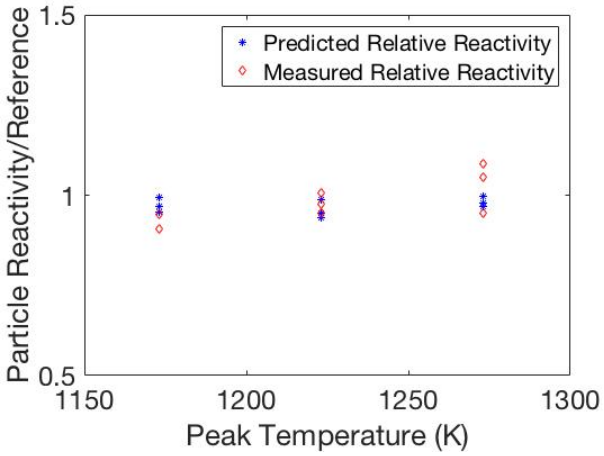

Figure 11. H_2O Annealing data and uncalibrated model predictions for an Indian Coal.

5.5. Model Implications

The literature indicates that the vast bulk of annealing occurs very rapidly, followed by a much more moderate loss of reactivity due to heat-treatment. The model described here has been designed to reflect this trend, which is thought to be due to initial, dramatic annealing during pyrolysis, and a lesser degree of annealing during subsequent heat-treatment. The annealing model therefore offers flexibility (when employed in a comprehensive coal conversion model) to allow char combustion predictions over a broad array of combustion conditions. However, no effective, coal-general kinetic correlation exists, so data are generally required to tune coal conversion rate constants. If data are available to tune kinetic constants, the initial annealing effects are embedded in the data, while the subsequent annealing effects may or may not be negligible, depending on coal type and combustion conditions. Thus the annealing model may be circumvented entirely in certain conditions, but is of considerable utility in comprehensive coal conversion models. In particular, the model shown here has been successfully employed in just such a comprehensive model to explain data over a broad range of conditions.[55]

Perhaps even more importantly, the literature data used in this work clearly show several orders of magnitude in char reactivity change due to char preparation condition, and both the data and the model show trends (at high T_{peak}) of converging char reactivities for diverse precursors. The historical failure of coal-general kinetic correlations has depended in large part upon many orders of magnitude of variation in the body of literature data between char reactivities, while no truly consistent pattern between proximate and ultimate analysis and char reactivity is readily discernible. The enormous impact of preparation condition on char reactivity (and the great

inconsistency in char preparation methods in the literature) certainly account for a portion of char reactivity variability. It is possible that preparation conditions even accounts for the bulk of observed variability, at least at practical (high T_{peak}) combustion conditions. If so, the present annealing model could potentially account for the preparation condition variability, and allow for a coal-general kinetic correlation based on structural parameters and/or the proximate/ultimate analysis.

6. Summary and Conclusions

A thermal annealing model functional form was developed based on observations supported by multiple authors, experimental methods, and detection systems. Qualitatively, coal char annealing is found to depend heavily on the time-temperature profile, the initial particle heating rate, the peak particle temperature, and the parent coal chemical structure as indicated by the NMR parameters. Trends in functional form dependence were quantified by optimizing a number of model forms for the annealing activation energy distribution to fit a broad array of literature data. The resulting model was shown to be a significant improvement; average error decreased to roughly a factor of two rather than a factor of five as compared to the preceding annealing model. The improvement is largely due to a model form that accounts for coal chemical structure, heating rate, and T_{peak}, as well as a much larger data set. Note that both the predicted degree of annealing, and the annealing activation energy distribution depend heavily on heating rate, T_{peak}, and chemical structure. Model functional dependency on HR and T_{peak} were previously included implicitly in the model form, which integrated a reaction rate at a specific temperature for a relevant increment of time. However, a more realistic model must

incorporate explicit dependence of the annealing activation energy distribution on HR, T_{peak}, and chemical structure. For example, ash fusion occurs solely as an effect of T_{peak}. Ash fusion in turn affects several annealing and char conversion pathways, such as catalyzing carbon crystallite rearrangement. If the ash fuses, a catalytic annealing pathway is eliminated, and the distribution of activation energies should shift accordingly. Similar arguments can be made for other annealing effects such as devolatilization, coal morphology, and coal precursor.

The annealing model was trained by a selection of 25 different data sets and 167 data points. Some data sets were initially excluded to test model predictivity; the model was found to predict the excluded data approximately as well as the training data. The model shows rapid decreases in char reactivity during heat-up and devolatilization before significant char oxidation occurs, and generally matches the decrease in reactivity best at temperatures above 1200 K (and especially above 1800 K), which was expected. The dependence on coal type was modeled using a chemical structure parameter measured by solid-state NMR spectroscopy.

While the average error factor was greatly reduced, much of the remaining error is due to a relatively few outliers with data at low values of T_{peak}. The weaker model results at low temperature are thought to be due to both greater diversity and poorer char characterization (i.e., annealing is far from complete, and the chars may have unfused ash, catalytic effects, residual volatiles, greater crosslinking etc.). Bearing in mind the disproportionate error in low-temperature experiments, and given that practical combustion occurs are temperatures in the range of ~2000-2300 K, the annealing model presented here works especially well in practical circumstances.

It was shown that annealing data relevant to CO_2 gasification is predicted at an acceptable level by the annealing model trained from O_2 oxidation reactivity data. This result is somewhat surprising as the limited literature data imply that O_2, CO_2, and H_2O active sites may all be different.[29] However, because current knowledge of coal reaction pathways is woefully incomplete, this result is certainly not impossible. The single set of available H_2O gasification data (with sufficient recorded experimental detail for this model), is also predicted quite well by the annealing model trained to O_2 oxidation data.

Despite model improvements, there is still considerable work that could be done to improve the annealing model. Such work includes data for an even broader array of coals, data collected over a large range of temperatures and heating rates with very short treatment times, and data that allow more detailed predictions of the initial time-temperature profile (prior to a fixed temperature soak time). There are also numerous other questions of interest that may prove more difficult to address. These questions include disentangling the coal swelling models and pore development from thermal annealing, a broader study of char ash content on thermal annealing (examining both ash quantity and chemical identity), and further investigation into early and late burnout effects. Late burnout effects are not related to annealing, but tend to obscure char reactivity (for example pore networks that are initially blocked during the metaplast phase, but may become unblocked even at a low level of char conversion).

Finally, it should be emphasized that this annealing model, like most prior literature models, impacts only the conversion rate law preexponential factor by decreasing the number of active sites available. It was implemented directly in a comprehensive coal char conversion model with

the parameters derived in this work (with a remarkable level of success).[55] However, the comprehensive model typically requires that key kinetic parameters be fit to data, since it lacks an effective coal-general reactivity correlation. This is a universal weakness in char conversion models, and it should be noted that the annealing model will impact the preexponential factor, so optimization or regression of kinetic coefficients for any char conversion model should take place *after* implementing the char annealing model.

Acknowledgements

The authors would particularly like to acknowledge Drs. Osvalda Senneca and Piero Salatino both for their significant quantities of published, relevant data and their willingness to discuss the details of their experiments.

This material is based upon work supported in part by the Department of Energy, National Nuclear Security Administration, under Award Number DE-NA0002375.

Funding for this work was provided by the Department of Energy through the Carbon Capture Simulation Initiative (CCSI) and the Carbon Capture Simulation for Industry Impact ($CCSI^2$) projects.

Los Alamos National Laboratory is operated by LANLS, LLC for the NNSA of the U.S. DoE under contract No. DE – AC52-06 NA 25396.

Disclaimer

References

1. Wall, T.; Liu, Y. H.; Spero, C.; Elliott, L.; Khare, S.; Rathnam, R.; Zeenathal, F.; Moghtaderi, B.; Buhre, B.; Sheng, C. D.; Gupta, R.; Yamada, T.; Makino, K.; Yu, J. L., An overview on oxyfuel coal combustion-state of the art research and technology development. *Chemical Engineering Research & Design* **2009,** 87, (8A), 1003-1016.
2. Scheffknecht, G.; Al-Makhadmeh, L.; Schnell, U.; Maier, J., Oxy-fuel coal combustion-a review of the current state-of-the-art. *International Journal of Greenhouse Gas Control* **2011,** 5, S16-S35.
3. Holland, T.; Fletcher, T. H., Global sensitivity analysis for a comprehensive char conversion model in oxy-fuel conditions. *Energy & Fuels* **2016**.
4. Senneca, O.; Salatino, P., Loss of gasification reactivity toward o-2 and co2 upon heat treatment of carbons. *Proceedings of the Combustion Institute* **2002,** 29, 485-493.
5. Nagle, J.; Strickland-Constable, R. F. Oxidation of carbon between 1000°c and 2000°c, *Fifth Carbon Conference*, Pennsylvania State University, Macmillan, Ed. Pergamon Press: Pennsylvania State University, 1962; 1, p 154.

6. Beeley, T.; Crelling, J.; Gibbins, J. R.; Hurt, R.; Lunden, M.; Man, C. K.; Williamson, J.; Yang, N. Y. C., Transient high-temperature thermal deactivation of monomaceral-rich coal chars. *Proceedings of the Combustion Institute* **1996**, (26th), 3103-3110.
7. Jenkins, R. G.; Nandi, S. P.; Walker, P. L., Reactivity of heat-treated coals in air at 500 degrees c. *Fuel* **1973,** 52, (4), 288-293.
8. McCarthy, D. J., Some effects of overheating and carbon burn-off on the performance of fluidized-bed combustors. *Fuel* **1982,** 61, (3), 298-302.
9. Radovic, L. R.; Walker, P. L.; Jenkins, R. G., Importance of carbon active-sites in the gasification of coal chars. *Fuel* **1983,** 62, (7), 849-856.
10. Suuberg, E. M.; Wojtowicz, M.; Calo, J. M., Some aspects of the thermal annealing process in a phenol-formaldehyde resin char. *Carbon* **1989,** 27, (3), 431-440.
11. Senneca, O.; Russo, P.; Salatino, P.; Masi, S., The relevance of thermal annealing to the evolution of coal char gasification reactivity. *Carbon* **1997,** 35, (1), 141-151.
12. Sahu, R.; Levendis, Y. A.; Flagan, R. C.; Gavalas, G. R., Physical-properties and oxidation rates of chars from 3 bituminous coals. *Fuel* **1988,** 67, (2), 275-283.
13. Radovic, L. R.; Walker, P. L.; Jenkins, R. G., Effect of lignite pyrolysis conditions on calcium-oxide dispersion and subsequent char reactivity. *Fuel* **1983,** 62, (2), 209-212.
14. Senneca, O.; Salatino, P., Overlapping of heterogeneous and purely thermally activated solid-state processes in the combustion of a bituminous coal. *Combustion and Flame* **2006,** 144, (3), 578-591.
15. Senneca, O.; Salatino, P.; Menghini, D., The influence of thermal annealing on oxygen uptake and combustion rates of a bituminous coal char. *Proceedings of the Combustion Institute* **2007,** 31, 1889-1895.
16. Senneca, O.; Salatino, P.; Masi, S., Heat treatment-induced loss of combustion reactivity of a coal char: The effect of exposure to oxygen. *Experimental Thermal and Fluid Science* **2004,** 28, (7), 735-741.
17. Senneca, O.; Salatino, P.; Masi, S., The influence of char surface oxidation on thermal annealing and loss of combustion reactivity. *Proceedings of the Combustion Institute* **2005,** 30, 2223-2230.
18. Hurt, R. H.; Gibbins, J. R., Residual carbon from pulverized coal-fired boilers .1. Size distribution and combustion reactivity. *Fuel* **1995,** 74, (4), 471-480.
19. Cai, H. Y.; Guell, A. J.; Chatzakis, I. N.; Lim, J. Y.; Dugwell, D. R.; Kandiyoti, R., Combustion reactivity and morphological change in coal chars: Effect of pyrolysis temperature, heating rate and pressure. *Fuel* **1996,** 75, (1), 15-24.
20. Shim, H. S.; Hurt, R. H., Thermal annealing of chars from diverse organic precursors under combustion-like conditions. *Energy & Fuels* **2000,** 14, (2), 340-348.
21. Shibaoka, M.; Ohtsuka, Y.; Wornat, M. J.; Thomas, C. G.; Bennett, A. J. R., Application of microscopy to the investigation of brown-coal pyrolysis. *Fuel* **1995,** 74, (11), 1648-1653.
22. Senneca, O.; Salatino, P.; Masi, S., Microstructural changes and loss of gasification reactivity of chars upon heat treatment. *Fuel* **1998,** 77, (13), 1483-1493.
23. Feng, B.; Bhatia, S. K.; Barry, J. C., Structural ordering of coal char during heat treatment and its impact on reactivity. *Carbon* **2002,** 40, (4), 481-496.
24. Wang, W.; Thomas, K. M.; Poultney, R. M.; Willmers, R. R., Iron-catalyzed graphitization in the blast-furnace. *Carbon* **1995,** 33, (11), 1525-1535.
25. Salatino, P.; Senneca, O.; Masi, S., Assessment of thermodeactivation during gasification of a bituminous coal char. *Energy & Fuels* **1999,** 13, (6), 1154-1159.
26. Shurtz, R. Effects of pressure on the properties of coal char under gasification conditions at high initial heating rates. PhD Dissertation, Chemical Engineering, Brigham Young University, Brigham Young University, 2011.
27. Shurtz, R. C.; Fletcher, T. H., Coal char-co2 gasification measurements and modeling in a pressurized flat-flame burner. *Energy & Fuels* **2013,** 27, 3022-3038.
28. Hurt, R.; Sun, J. K.; Lunden, M., A kinetic model of carbon burnout in pulverized coal combustion. *Combustion and Flame* **1998,** 113, 181-197.
29. Liu, G. S.; Niksa, S., Coal conversion submodels for design applications at elevated pressures. Part ii. Char gasification. *Progress in Energy and Combustion Science* **2004,** 30, 679-717.
30. Feng, B.; Bhatia, S. K.; Barry, J. C., Variation of the crystalline structure of coal char during gasification. *Energy & Fuels* **2003,** 17, (3), 744-754.
31. Radovic, L. R.; Walker, P. L.; Jenkins, R. G., Effect of lignite pyrolysis conditions on calcium-oxide ddispersion and subsequent char reactivity. *Fuel* **1983,** 62, (2), 209-212.
32. McCarthy, D. J., Some effects of overheating and carbon bunr-off on the performance of fluidized-bed combustors. *Fuel* **1982,** 61, (3), 298-302.
33. Smoot, D. L.; Smith, P. J., *Coal combustion and gasification*. Plenum Press: New York, 1985; Vol. 1, p 443.

34. Holland, T. M. A comprehensive coal conversion model extended to oxy-coal conditions. PhD Dissertation, Chemical Engineering, Brigham Young University, Provo, UT, in progress 2017.
35. Genetti, D.; Fletcher, T. H.; Pugmire, R. J., Development and application of a correlation of c-13 nmr chemical structural analyses of coal based on elemental composition and volatile matter content. *Energy & Fuels* **1999,** 13, (1), 60-68.
36. Feng, B.; Jensen, A.; Bhatia, S. K.; Dam-Johansen, K., Activation energy distribution of thermal annealing of a bituminous coal. *Energy & Fuels* **2003,** 17, (2), 399-404.
37. Russell, N. V.; Gibbins, J. R.; Man, C. K.; Williamson, J., Coal char thermal deactivation under pulverized fuel combustion conditions. *Energy & Fuels* **2000,** 14, (4), 883-888.
38. Bar-Ziv, E.; Zaida, A.; Salatino, P.; Senneca, O., Diagnostics of carbon gasification by raman microprobe spectroscopy. *Proceedings of the Combustion Institute* **2000,** 28, 2369-2374.
39. Naredi, P.; Pisupati, S. V., Interpretation of char reactivity profiles obtained using a thermogravimetric analyzer. *Energy & Fuels* **2008,** 22, (1), 317-320.
40. Gale, T. K. Effects of pyrolysis conditions on coal char properties. M.S. Thesis, Mechanical Engineering, Brigham Young University, Provo, UT, 1994.
41. Gale, T. K.; Bartholomew, C. H.; Fletcher, T. H., Decreases in the swelling and porosity of bituminous coals during devolatilization at high heating rates. *Combustion and Flame* **1995,** 100, (1-2), 94-100.
42. Gale, T. K.; Bartholomew, C. H.; Fletcher, T. H., Effects of pyrolysis heating rate on intrinsic reactivities of coal chars. *Energy & Fuels* **1996,** 10, (3), 766-775.
43. Wu, S. Y.; Gu, J.; Zhang, X.; Wu, Y. Q.; Gao, J. S., Variation of carbon crystalline structures and co2 gasification reactivity of shenfu coal chars at elevated temperatures. *Energy & Fuels* **2008,** 22, (1), 199-206.
44. Jayaraman, K.; Gokalp, I.; Bonifaci, E.; Merlo, N., Kinetics of steam and co2 gasification of high ash coal–char produced under various heating rates. *Fuel* **2015,** 154, 370-379.
45. Zolin, A.; Jensen, A.; Dam-Johansen, K., Kinetic analysis of char thermal deactivation. *Proceedings of the Combustion Institute* **2000,** 28, 2181-2188.
46. Buch, T.; Guala, J. A.; Caneiro, A., Oxyreactivity of doped sucrose carbon. *Carbon* **1978,** 16, (5), 377-383.
47. Edwards, I. A. S., Chapter 1 - structure in carbons and carbon forms. In *Introduction to carbon science*, Butterworth-Heinemann: 1989; pp 1-36.
48. Sacks J., W., W.J., Mitchell, T.J. and Wynn, H.P. , *Statistical Science* **1989,** 4, 409-423.
49. Welch, W. J.; Buck, R. J.; Sacks, J.; Wynn, H. P.; Mitchell, T. J.; Morris, M. D., Screening, predicting, and computer experiments. *Technometrics* **1992,** 34, (1), 15-25.
50. Kennedy, M. C.; O'Hagan, A., Bayesian calibration of computer models. *Journal of the Royal Statistical Society Series B-Statistical Methodology* **2001,** 63, 425-450.
51. Gattiker, J., Myers, K., Williams, B., Higdon, D., Carzolio, M., & Hoegh, A. , Gaussian process-based sensitivity analysis and bayesian model calibration with gpmsa. In *Handbook of uncertainty quantification*, Ghanem, H., Owadhi, Ed. Springer: 2017; pp 1-41.
52. McKay, M. D.; Beckman, R. J.; Conover, W. J., A comparison of three methonds for selecting values of input variabls in the analysis of output from a computer code. *Technometrics* **1979,** 21, (2), 239-245.
53. Genetti, D. An advanced model of coal devolatilization based on chemical structure. M.S. Thesis, Chemical Engineering, Brigham Young University, Provo, UT, 1999.
54. Shurtz, R. C.; Kolste, K. K.; Fletcher, T. H., Coal swelling model for high heating rate pyrolysis applications. *Energy & Fuels* **2011,** 25, (5), 2163-2173.
55. Holland, T.; Fletcher, T. H., Comprehensive model of single particle pulverized coal combustion extended to oxy-coal conditions. *Energy & Fuels* **2017,** 31, 2722-2739.
56. Zolin, A.; Jensen, A.; Jensen, P. A.; Frandsen, F.; Dam-Johansen, K., The influence of inorganic materials on the thermal deactivation of fuel chars. *Energy & Fuels* **2001,** 15, 1110-1122.
57. Zolin, A. Reactivity of solid fuels. PhD Thesis, Chemical and Biochemical Engineering, Technical University of Denmark, Lyngby, Denmark, 2001.
58. Senneca, O.; Cortese, L., Thermal annealing of coal at high temperature and high pressure. Effects on fragmentation and on rate of combustion, gasification and oxy-combustion. *Fuel* **2014,** 116, 221-228.